MSc Biomedical Engineering

Bacterial adherence on 3-D printed plasma electrolytic oxidized titanium implants in dynamic conditions

Master Thesis

Ivo Frints

Delft University of Technology

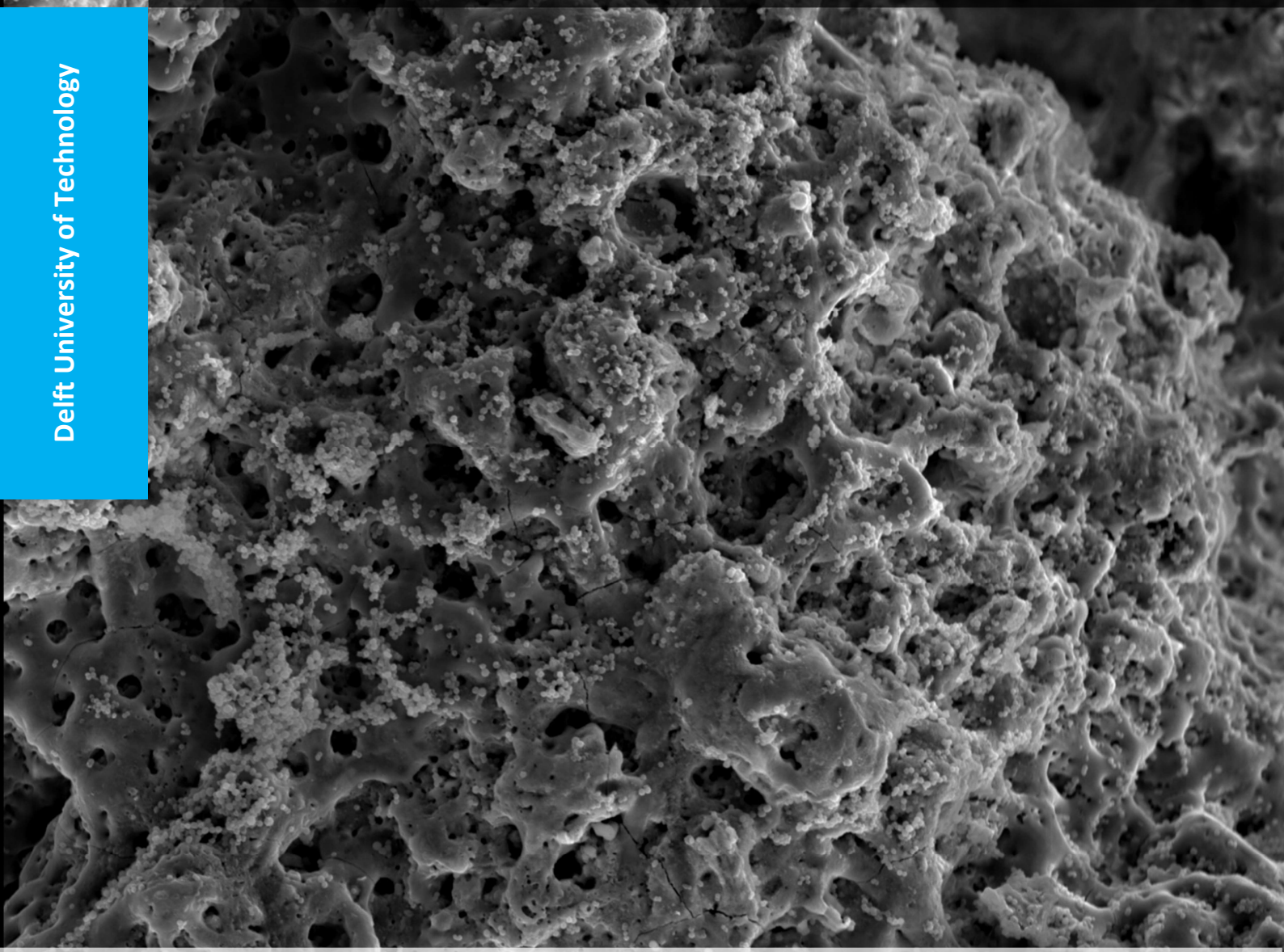

Supervision: Ir. Raymond Bevers
Dr. Chris Arts
Dr.ir. Iulian Apachitei
Prof.dr. Amir A. Zadpoor

Maastricht University

TU Delft Delft University of Technology

Bacterial adherence on 3-D printed plasma electrolytic oxidized titanium implants in dynamic conditions

By

Ivo Frints
4595459

In partial fulfilment of the requirements for the degree of:

Master of Science
in Biomedical Engineering

At the Delft University of Technology

To be defended on:
9 September 2020

Supervisors

ir. Raymond Bevers
Maastricht University Medical Center

Dr. Chris Arts
Maastricht University Medical Center

Dr. ir. Iulian Apachitei
Delft University of Technology

Prof.dr. Amir A. Zadpoor
Delft University of Technology

Thesis performed at the

Department of Orthopaedic Surgery
Maastricht University Medical Center+

&

Biomaterials and Tissue Biomechanics research group

Department of Biomechanical Engineering
Delft University of Technology

Abstract

Osteoarthritis, the degeneration of articular cartilage, which causes loss of mobility and chronic pain for patients is a common condition with high clinical demand. Care of this condition currently attributes to ±1.4% of the Dutch annual health care costs, but due to the rapidly aging Dutch population a 41% increase of cases is projected over the next 20 years. Treatment for the most frequently diagnosed forms of osteoarthritis, knee and hip respectively, involves the removal of damaged tissue and placing an artificial total joint replacement (TJR), restoring partial mobility and relieving pain. Despite its success and demand, annually 10% of these treatments are affected by infections or aseptic loosening, which combined with the increase of cases and rapid development of antibiotic-resistant bacteria requires drastic optimization.

Promising strategies that allow infection prevention while assisting the bone-implant fixation are currently in development, with the common approach consisting of bioactive coatings which enhance the currently applied implants with these antibacterial or bone growth related capabilities. One of these methods in development is the Plasma Electrolytic Oxidation (PEO), which additionally combines morphological changes and chemical biofunctionality by incorporating bioactive elements in the implants' surface layer. Until now, antibacterial surfaces bearing silver nanoparticles (AgNPs) have been incorporated into the surfaces of 3D printed titanium implants by PEO but their antibacterial properties have been studied only in static conditions.

This study aimed to further characterize the antibacterial effect of these implants by testing their efficacy against bacterial adherence in both dynamic and static conditions. The additive manufactured Ti-6Al-4V implants were biofunctionalized by PEO with added AgNPs at different concentrations, resulting in non-treated, PEO treated, PEO + 0.3 g/l AgNPs and PEO + 3.0 g/l AgNPs implants. These implants were characterized to relate these to previous PEO implant related studies. During this study, the Centers for Disease Control and Prevention (CDC) bioreactor model was adjusted to fit these PEO + AgNPs implants and test them in conditions of bacterial adherence. Robustness and bacterial adherence were optimized for this adjusted method, where despite thorough troubleshooting inconsistent behaviour was found in the bacterial concentrations in the reactor media in an illogical manner. Dynamic conditions of this reactor caused by the fluid flow were analysed by simulation, this resulted in a calculated shear stress of 0.0058 dynes/cm^2, akin to the lower limit magnitude of shear stresses caused by interstitial fluid. Despite shortage of results due to the omitted inconsistent experiments combined with the lost data due to force majeure (COVID-19), a higher bacterial adherence was examined in dynamic conditions compared to static conditions.

Acknowledgements

Over the last year, as part of the internship and literature review, I have been allowed to investigate methods to assist implant development by *in vitro* characterization of their bone assisting and infection preventing capabilities. During this period approaching the thesis there have been unintentional delays and shifts in research due to roadblocks caused by logistical limitations, ultimately narrowing the thesis research down on the current topic.

The product before you was successfully developed despite all ups and downs, for which I´d like to express my gratitude to all who were, conscious or subconsciously, instrumental support to me during this project.

In no particular order, I´d like to thank my graduation supervisor Dr. ir. Iulian Apachitei [TU Delft] for his guidance through the graduation processes, understanding and allowing me to pursue a project within research and development of novel implants in collaboration between the Biomaterial department of TU Delft and the Orthopaedic research department of Maastricht UMC+. I appreciate your continued support and availability, not only during the thesis but also during the master as Coordinator of Biomedical Engineering and the Biomaterials track from when I started this master mid- academic year.

I would like to similarly explicitly thank my thesis supervisor ir. Raymond Bevers [MUMC+] for allowing me to be pioneer of the research and strategies. I would like to express my additional gratitude for the numerous discussions of possibilities, brainstorms on optimization, critical feedback, celebration of progress and the great collegiality and teamwork we had. Additionally, I would like to thank Dr. Chris Arts [MUMC+] for his advice and directions during the key meetings together with my thesis supervisor.

Thanks also goes to Erik Beuken who was instrumental in the setup of microbiologic research at the MUMC+ microbiology department. Similarly, I would like to thank Sander Leeflang, Ingmar van Hengel and Niko Eko Putra for their insights and assistance during the biofunctionalization of implants and related experiments at the Biomaterials and Tissue Biomechanics research group of TU Delft.

To all my colleagues, including the fellow students, of the Orthopaedic Research Department of MUMC+ I would like to express my gratitude for the valuable experiences, shared knowledge and all the fun moments.

Special gratitude, which is difficult to elaborate, goes to my parents who were on my team from day zero and have never stopped being there.

To finish, I would like to thank my friends and loved ones, especially Celine, for their invaluable love and support during my study and thesis process.

Ivo Frints

Maastricht
June 2020

Contents

Table of Figures

Nomenclature

Anode;
: Positively charged electrode where electrons leave an electrical device, counterpart to a cathode

Articular cartilage;
: The smooth white tissue that covers the ends of bones where they come together to form joints

Aseptic loosening;
: Failure of the bond between an implant and bone in the absence of infection.

Bacterial adherence;
: Generally irreversible fixation of implants on a surface in the beginning of colonization.

Bioactive/ bio-functional;
: The characteristic of having a biological effect.

Bioreactor;
: A device that supports a biologically active environment.

Cathode
: Negatively charged electrode where electrons enter an electrical device, counterpart to an anode

Dynes/cm^2 = 10^{-1} Pa
: Smaller unit of pressure.

Eppendorf tube
: Single use polypropylene tubes used for preparing, mixing, centrifuging, transporting and storing solid and liquid samples and reagents.

Interstitial fluid;
: The thin layer of fluid surrounding the body's cells.

Morphological;
: Related to the form, structure and structural features

Chapter 1 Introduction

1.1 Osteoarthritis in the Netherlands, its treatment, and complications

Osteoarthritis is the condition where articular cartilage or bone ends are deteriorated in such severity where this leads to stiffening, loss of flexibility and/or chronic pain. In the Netherlands the number of osteoarthritis cases has been constantly rising for the past decade with 31 thousand hip and 49 thousand knee cases diagnosed in 2018 [2]. For treatment and care of this, in 2017 their associated annual costs were at 488 and 433 million euro which combined to 1.1% of the total annual Dutch healthcare expenses and are increasing together with the number of cases [2, 3]. With currently no cure available, the relief of pain and joint functionality is instead restored by total joint replacement (TJR). Around 30 thousand procedures of both hip and knee TJRs were performed in 2018 where osteoarthritis was diagnosed as main condition for these procedures at 97.6% and 87.3% for the hip and knee TJR, respectively [4]. During the implant placement and subsequent patient recovery there are risks of aseptic loosening and implant-related infections compromising the implant, its functionality and the patients' health [5-9]. Risk of infection increases with the duration of open surgery, while aseptic loosening risks are related to endothelial dysfunction, physical irritation or local inflammatory reactions [6, 8, 10]. Out of the 68 thousand hip/knee TJRs performed in the Netherlands in 2018, 10% were revision surgeries with aseptic loosening and infections as major causes [4]. These current implant failure rates, combined with the prospect of an 41% increase of osteoarthritis cases over the next 20 years due to the aging Dutch population, cements the need for cost effective solutions for less complication sensitive treatments [11].

1.2 Strategies to prevent infections

Current prevention of infection on or around the implants, the peri-prosthetic joint infections (PJIs) or implant-associated infections (IAI), occurs by disinfection on and around the area of incision, limiting incision size, duration of the open surgery and administering of local and systemic antibiotics. Despite these pre-emptive measures there is an infection prevalence of 2% for the Dutch hip/knee TJIs[4]. This current rate combined with rapid development of antibiotic-resistant bacteria, such as the common PJI causing methicillin-resistant Staphylococcus aureus (MRSA), and general increase of osteoarthritic cases there is a high necessity of additional and improved methods of infection prevention [12].

These infections commonly occur due to the migration of commensal bacteria, such as Staphylococcus aureus/epidermis on the skin or Pseudomonas aeruginosa from the nose, to the open wound where the immune system is compromised and the bacteria could adhere to the implant surface [13-16].

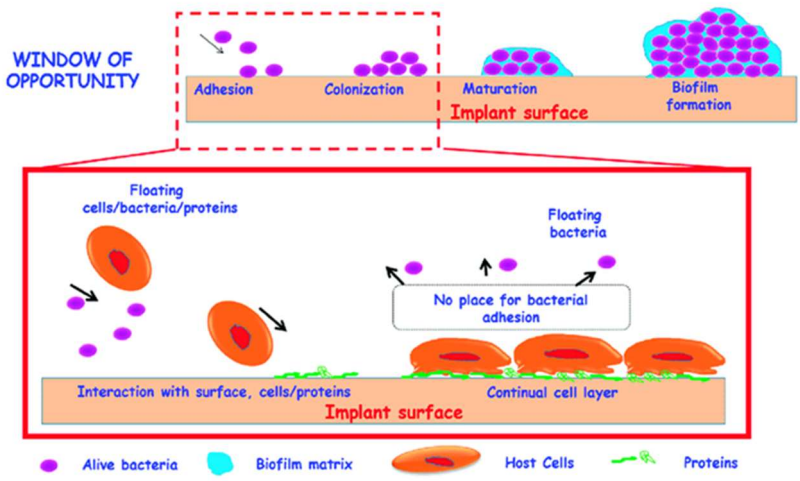

Figure 1. Implant adherence and biofilm formation [1].

From the point of adherence, the bacteria will continue growing, colonizing the surface to develop a biofilm, such a biofilm provides a layer of antibacterial resistance and hinderance of bone apposition, subsequently resulting in septic loosening (Figure 1) [17, 18].

In prevention of implant failure, the common strategy has been modifying implant surfaces such that mechanical properties are preserved while biofunctional additives are added. Multiple additives are or have been studied but are either still in development or had shortcomings that required re-evaluation. Antibacterial modifications strategies included for instance: antibiotics, inorganic nanoparticles and ions, and anti-adhesion coatings [19]. The benefit of surface modifications is that bone growth can be enhanced while simultaneously inhibiting the bacterial adherence. One of these latter coupled approaches currently in development is a form of surface modification which utilizes both the morphologic and chemical characteristics of the treatment, combining the two in a single layer. This layer is synthesized by oxidizing the implant surface by PEO, where high voltage sparks are distributed over the surface of the metallic material at high frequency, transforming it to a roughened surface with micro/nano porous crater like features [20-22]. One of the advantages of this porous oxide layer is that antibacterial inorganic (e.g. zinc or silver) nanoparticles, osteogenic (e.g. Strontium or Calcium), or other biofunctional agents can be incorporated in the oxide layer [20-22].

1.3 Development limitations of biomaterial strategies

Numerous potent infection prevention methods such as the PEO surface biofunctionalization are under development, but the path from a novel method towards clinical application easily takes 7+ years and generally follows the procedure indicated in Figure 2 [23]. A majority of this goes into both preliminary research and the extensive animal and human trials which are the most important but also time and cost consuming aspects of development [24, 25]. Despite necessity of human trials prior to product launch, optimization or minimization of these would yield time and cost reductions. To a certain degree, *in vitro* characterization is therefore the commonly used method to study the properties of the implants during the development phase [26].

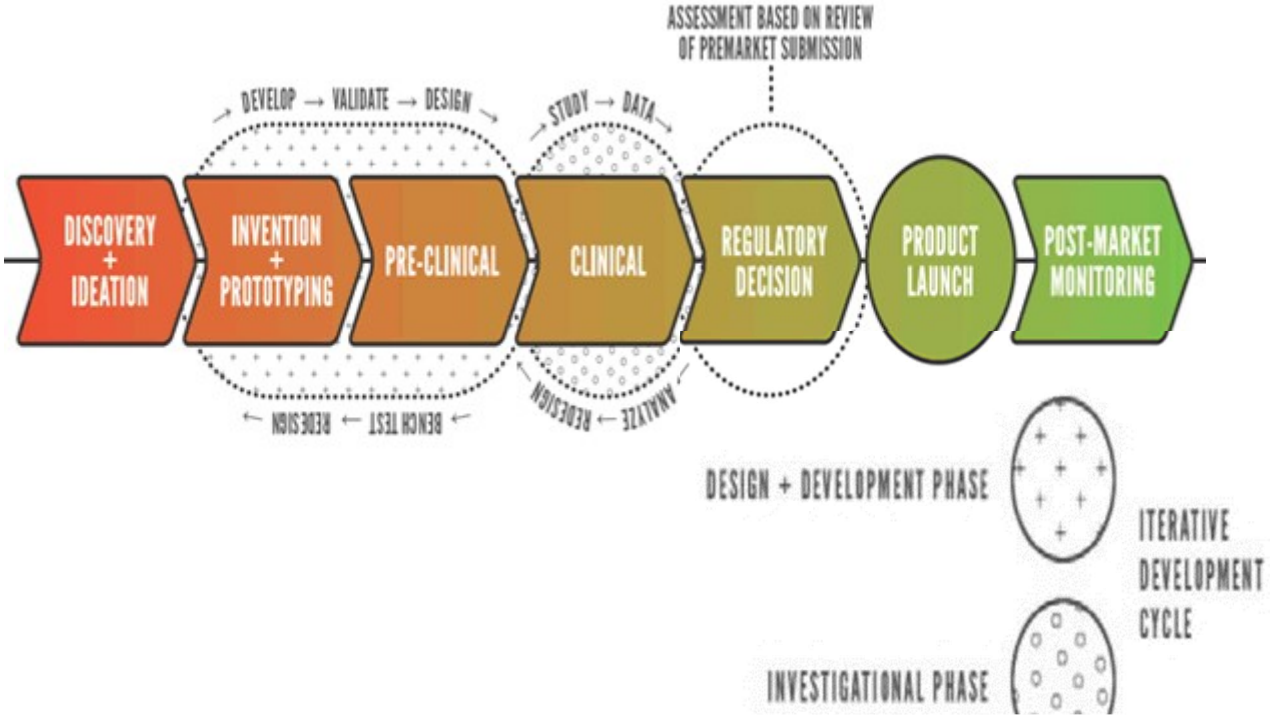

Figure 2. Medical device development pathway [27].

There are however multiple approaches to study the properties and infection preventing effects of the novel strategies, which to varying degrees exclude representation of bodily conditions due to

pragmatic or logistic reasons [19]. While this allows quick and repeatable analysis of the fundamental properties, which is invaluable in early development stages, the introduction of elements more representative of human physiology might drastically change the results analysed for these characteristics. A common example for this is the experiments performed in static conditions, compared to those in which dynamic elements such as fluid flow, nutrient-/waste exchange, or co-culture aspects were added. Both have their intrinsic differences in complexity, time, relevance to physical conditions and repeatability, making it such that dynamic experiments would logically follow on fruitful static ones and precede the animal (and human) trials.

Considering the implants biofunctionalized by PEO, numerous assays have been performed. Despite this, the mechanism of adherence, biofilm and infection prevention had not yet been analysed in a dynamic environment for these implants incorporated with AgNPs.

1.4 Aim of the study

This study aims to compare the bacterial adherence of the Ti implants bearing AgNPs in static conditions to their adherence in dynamic conditions. To this end, Ti-6Al-4V implants were first additive manufactured by selective laser melting and then biofunctionalized with different concentrations of AgNPs by PEO process. The implants were characterized with respect to their surface morphology, chemical composition, silver ion release and antibacterial capabilities. To perform the dynamic experiments an additional aim was to adjust an existing bioreactor model such that it fit the study design while achieving robustness and consistency of bacterial adherence. Finally, the dynamics of the model were investigated and compared to *in vivo* shear conditions by simulating the respective model and calculating the expected shear forces.

1.5 Bioreactor model adjustment

A method for bacterial adherence in dynamic conditions was developed during this study by adjusting the CDC biofilm reactor model (Biosurface Technologies, Montana, USA) to fulfil the requirements of the study design. The original model was developed to grow and test microbial biofilm under moderate to high shear dynamics with an option of continuous flow. This robust and validated reactor model, incorporated in ASTM E2562 and ASTM E3161, has been used with different bacteria, materials and for various aspects of biofilm research such as biofilm detection, biofilm structure analysis, biofilm growth dynamics and antimicrobial agent – biofilm interactions [28-37]. For this study, the CDC biofilm reactor model and process were adjusted to fit the implants and facilitate adherence without biofilm formation and was experimentally tested. During the bacterial experiments in both dynamic and static procedures the SA113 (ATCC 35556) Staphylococcus aureus (*S.aureus*) strain was utilized, due to its proven bacterial adherence and biofilm formation capabilities, Staphylococcus prevalence in PJIs/IAIs and in-house experience with the strain [38-40]. The resulting design, process modifications and troubleshooting of the custom bioreactor setup are incorporated and presented in this study.

Chapter 2 Materials and Methods

2.1 Ti-6Al-4V mouse femur implants

The implants used in this study were previously developed [22] for a mouse femur model. The design criteria for these provided the design with porosity (to maximize the biomaterial's bone ingrowth and fixation), appropriate diameter to fit murine femurs (for assessment of *ex vivo* antimicrobial activity, Figure 3) and re-producibility by additive manufacturing [20-22].

These cylindric implants (Figure 4) were 40 mm in length and ∅ 0.5 mm thick. They were manufactured according to the pre-established design at the Additive Manufacturing Lab (TU Delft, Delft, The Netherlands). In brief, this production entailed melting medical-grade Ti-6Al-4V powder using an SLM machine (SLM-125, Realizer, Borchem, Germany) equipped with an Ytterbium fibre laser under inert atmosphere with an oxygen content below 0.2% [20-22].

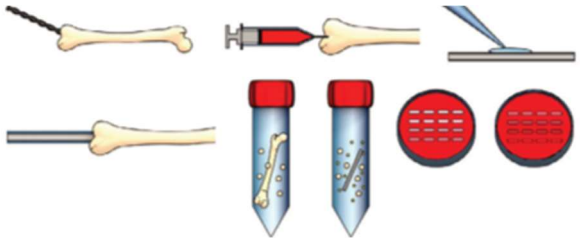

Figure 3. Mouse femur model schematic [21].

Figure 4. Implant design [22].

2.2 Surface biofunctionalization

2.2.1 Setup

Plasma electrolytic oxidation process is performed using the setup schematically shown in Figure 5. The setup comprised of an AC power supply (50 Hz, type ACS 1500, ET Power Systems Ltd, Eyam, England), computer interface (SCXI, National Instruments, Austin, Texas, United States), cooling system (Thermo Haake, Karisruhe, Germany), magnetic stirrer (IKA-Werke GmbH & Co. KG, Staufen, Germany), ring-shaped stainless steel cathode, and the double walled electrolytic cell, in which the surface synthesis will take place (Figure 6).

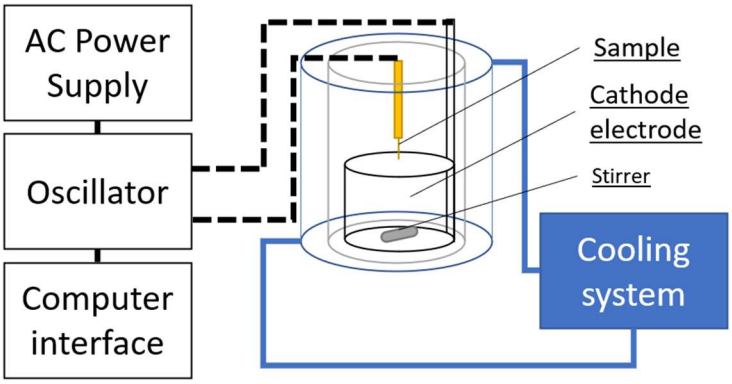

Figure 5. PEO setup, schematic representation.

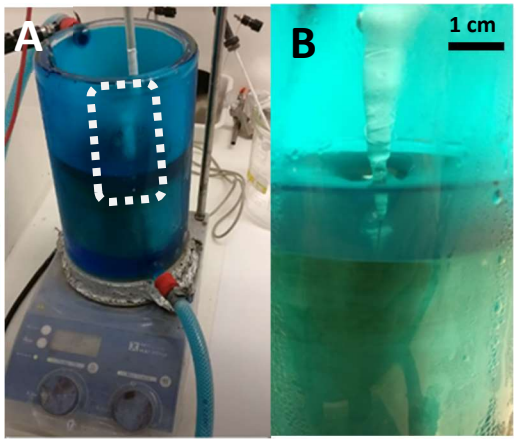

Figure 6. Double-walled glass electrolyte beaker with mounted Ti-6Al-4V implant. (A) Overview. (B) Enlarged view in A.

2.2.2 Preparation

Prior to the surface treatment the SLM implants were vacuum cleaned, to remove the powder remnants, thereafter ultrasonicated in acetone, 96% ethanol and demineralized water for 5 min each for further cleaning.

The PEO electrolyte was prepared by dissolving 24 g/l calcium acetate (≥99%, Sigma-Aldrich, St. Louis, Missouri, United States) and 4.2 g/l calcium glycerophosphate (≥99%, Dr Paul Lohmann GmbH, Emmerthal, Germany) in demineralized water by stirring. An overview of the samples used is presented in Table 1. For the respective sample groups (Table 1) the corresponding concentration of spherical AgNPs of 7 – 24 nm diameter (Sigma-Aldrich, St. Louis, Missouri) was added. After addition of the nano particles, the electrolyte was ultrasonicated twice for 5 min with a 5 min stirring at 500 rpm in between for a better dispersion of AgNPs. Per electrolyte solution no more than 20 implants were treated.

During the electrolyte preparation the double walled electrolytic cell was cooled at about 6°C by setting the cooling system to 0°C. An 800 ml electrolyte solution was prepared and poured into the cell, after which the cell and its contents were continuously cooled and stirred at 500 rpm on a magnetic stir plate. After reaching the temperature of 6°C the PEO procedure was initialised by mounting a previously PEO treated Ti-6Al-4V sample in the setup and running a current over the now formed circuit between the cathode ring, the electrolyte solution and the mounted disc which functions as anode. Based on this procedure the applied current was adjusted until a current density of 20 A/dm^2 was reached, which for the implants used in this study was equivalent to 0.39 A.

Table 1. Experimental groups used in this study

Group name	Description
NT	*Control* Ti-6Al-4V implants as manufactured
PEO	*PEO control* Ti-6Al-4V implants PEO treated
0.3 Ag	*Low silver PEO group,* Ti-6Al-4V implants PEO treated + 0.3 g/l AgNPs inclusions
3.0 Ag	*High silver PEO group,* Ti-6Al-4V implants PEO treated + 3.0 g/l AgNPs inclusions

After setting up the current, the disc was swapped for an implant, performing the surface treatment when the 6°C temperature was reached. Each implant was oxidized for 5 min at 0.39 A. During the PEO experiments, the resulting “voltage – time” data was recorded.

After treatment, each implant was flushed with demineralized water and air dried. Then, the samples were cut to lengths of 10 mm and 20 mm, respectively and stored in glass jars. All samples were sterilized by autoclaving for 1h at 110°C.

2.3 Implant characterization

2.3.1 Surface morphology and chemical analysis

The implant surface was morphologically and chemically analysed by scanning electron microscopy (SEM) and energy dispersive X-ray spectroscopy (EDS). Samples (n = 1 per group) were prepared by fixating 10 mm cut implants using conductive carbon tape and gold sputtering these for 30 seconds to improve their electrical conductivity. Prepared samples were mounted and analysed in the SEM (JSM-IT100LV, JEOL, Tokyo, Japan), set to a working distance of 10 - 11 mm and an electron beam energy of 15 kV.

2.3.2 Ag ion release

For the 0.3 Ag and 3.0 Ag implant groups the release of Ag ions was measured with inductively coupled plasma optical emission spectrometry (ICP-OES). This was performed by placing 10 mm cut implants (n = 3 per group) in dark Eppendorf tubes filled with 1 ml phosphate buffered saline (PBS) and storing these at 37°C. Samples were collected after 3, 6, 12 and 24 h and stored at 4°C. After dissolving the ions by adding 7 ml nitric acid (70%) the Ag concentrations were measured with the PerkinElmer Optima 3000DV (PerkinElmer, Zaventum, Belgium), subsequently the measurements were adjusted for the nitric acid dilution and the multiple timepoints provided a stepwise cumulative ion release.

2.4 Dynamic adherence reactor design and experiment adjustments

Standard polypropylene CDC biofilm reactor rods purchased from Biosurface Technologies (Montana, USA) designed to hold discs (12.7 mm) were shortened and slotted to hold novel inserts. Custom modular inserts were designed and manufactured to fit the model and allow the 20 mm implants to be mounted with 10 mm exposed to the bioreactor dynamics. The modified CDC-reactor model was equipped with two custom holders, each bearing 2 implants, sealing the additional sample holder slots with biologically inert silicone stops. Flow perfusion elements present in the general CDC bioreactor design were omitted for this adherence focused study, with the experiment duration and media contents adjusted similarly.

Consistency of results was achieved through iterative optimization of the custom bioreactor setup. Multiple experiments were performed (Table 2), readjusting the next experiment parameters based on the outcomes. Aspects such as potential cleaning remnants, temperature control and effect of media and bacterial concentration were all taken into account to improve consistency of results and limit the loss of bacteria.

Table 2. Trials to optimize the custom bioreactor setup and allow bacterial adherence on the non-PEO treated implants after dynamic incubation (20h, 37°C, 125 rpm)

T1	**Media; 10%TSB supplemented PBS; CFU/ml after inoculation; ± 3 x 10^5, 6 Ti-6Al-4V discs**
T2	Blank run, results omitted
T3	Media adjusted → 2.5mg/ml D-glucose supplemented PBS Samples adjusted → 6 Ti-6Al-4V discs in standard holder + 4 Ti-6Al-4V implants in custom holder
T4	Repetition of **T3** with reactor media incubated in shake incubator in parallel to run
T5	Repetition of **T3,** increased water rinses after chlorine deactivation, temperature logged
T6	Repetition of **T5**
T7	Repetition of **T5**, omission of samples, stirring mechanism and stirring
T8	Repetition of **T7**, reintroducing stir mechanism set to 125 rpm
T9	Repetition of **T8**, CFU/ml after inoculation adjusted → ± 6 x 10^6
T10	Repetition of **T9,** reintroducing 4 Ti-6Al-4V implants in custom holder, no temperature logs
T11	Repetition of **T10**, improved removal of non-adherent bacteria
T12	Repetition of **T10**, with 3.0 g/l AgNPs PEO treated implants

2.5 Fluid dynamics and shear force analysis

Local fluid shear stresses experienced by the implants were simulated using the COMSOL Multiphysics v. 5.4 software (COMSOL AB, Stockholm, Sweden). The modelling of the dynamics and geometry was based on the Mixer Module "Mixer" application and was adjusted to the reactor's geometry according to its dimensions (Figure 7.ABC) [41]. Media characteristics simulated using the Zetasizer mixture analysis software (Spectris, Surrey, United Kingdom) for PBS + 2.5 mg/ml glucose at 37°C, which resulted in dynamic viscosity of 0.6725 mPa·s. Shear rate was determined for the implants' location, and would for this Newtonian fluid relate to shear stress in the relation of Equation 1, in which τ is the

shear stress in [Pa], γ̇ is shear rate in [1/s] and η is the dynamic viscosity [Pa·s] according to the Newtonian law of viscosity [42].

Equation 1. Newtonian law of viscosity

$$\tau = \dot{\gamma} * \eta$$

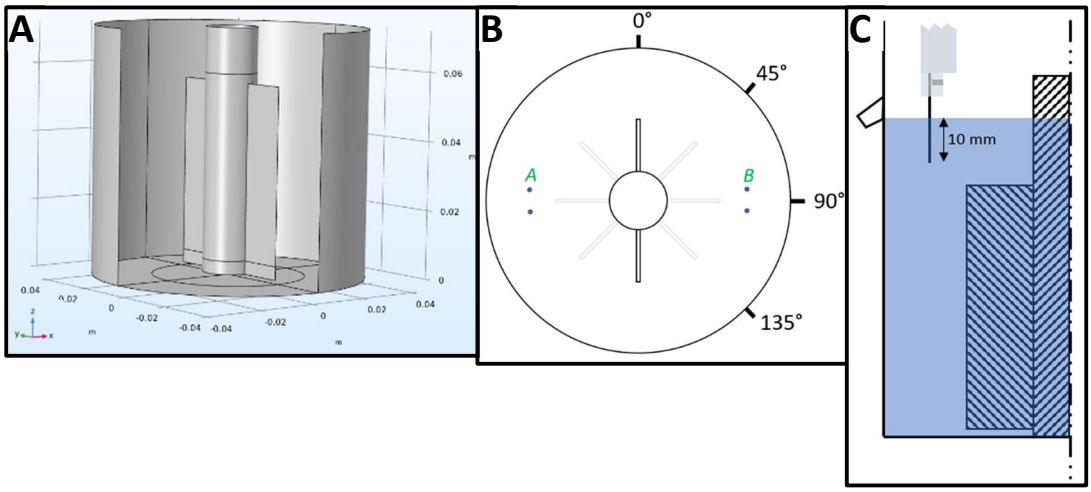

Figure 7. Geometry and design of the modelled Bioreactor (A) Simulated model. (B) Stir blade angle orientations. (C) Implant placement in the reactor.

2.6 Bacterial experiments

2.6.1 Stock preparation

Antibacterial effect and bacterial adherence were evaluated with a bacterial inoculum of the biofilm forming Staphylococcus Aureus strain SA113 (ATCC 35556) [38, 39]. This strain was aerobically grown in 5 ml Tryptic soy broth (TSB) incubated at 37°C overnight on a shake plate @ 160 rpm. Subsequently the culture was centrifuged (10 min x 21°C at 3000 rpm) such that a cell-pellet was formed. The stock culture was generated by discarding the supernatant TSB and resuspending the cell-pellet in 5 ml PBS. Bacterial concentration of this stock culture was measured by colony forming unit (CFU) count and found to be ± 3 x 10^8 colony forming units per ml (CFU/ml) which for experimental purposes remains constant for 3 weeks when stored at 4°C. Assay specific inocula were prepared from this stock.

2.6.2 Reactor preparation and assembly

Assembly of the bioreactor takes place after the components are correctly sterilized (Table 3). Parts in direct contact with the bacterial solution were deactivated by a 30 min drench in chlorine at 1500 ppm after which they were thoroughly flushed with demineralized water. Together with the components not directly contaminated these were then drenched and wiped with 70% ethanol covering all surfaces.

Table 3. Disinfection procedure of reactor components

Component	Procedure
Implants	Autoclave at 121°C for 1h
-Reactor vessel -Tubing	1500 ppm chlorine drench for 30 min → Demineralized water drench/rinse for 15 min → 70% Ethanol wipe for 30 sec → air dried → Autoclaved at 121°C for 1h
-Stir mechanism	1500 ppm chlorine drench for 30 min → Demineralized water drench/rinse for 15 min → 70% Ethanol wipe for 30 sec → air dried
-Implant holder -Reactor lid -Lid stops	70% Ethanol drench for 5 min, wiped → air dried

After evaporation of ethanol remnants the model was assembled in the experiment's class 1 laminar air flow cabinet wearing gloves. Lid openings were fitted with silicone stops and the stir assembly was re-assembled (Figure 8.A). Subsequently these were placed on the autoclaved reactor vat while the autoclaved tubing was connected to the outlet with its pinch valves closed (Figure 8.B). Media was added by temporarily removing one of the stops and funnelling in 1250 mg D-Glucose followed by 500 ml autoclaved PBS. The vat with contents was stirred at 125 rpm and brought to 37°C on a heated stir plate mounted on a spill box (Figure 8.C). After fully dissolving the D-glucose the outlet was temporarily opened disposing excess media, 9 ml of this excess media was collected as inoculum reagent and brought to the designated microbiological lab. Inoculum was prepared by resuspending 1 ml of 10-fold concentrated stock solution in the 9 ml brought PBS. A concentrated stock reaching ± 3 x 10^9 CFU/ml was prepared similar to the ordinary stock, with the change of growing the bacteria in 50 ml instead of 5 ml TSB, centrifuging and resuspending was performed as described in the stock preparation.

Figure 8. Assembly of the reactor. (A) Lid and stir mechanism. (B) Reactor and waste tubing. (C) Placement on top of stir plate.

For sample preparation two sterile implants were mounted per disinfected holder (n = 2 holders per experiment). Tweezers, disinfected with 70% ethanol, were used to pick up the implant such that the top 10 mm remained undisturbed, then the shortest extending end was placed in the holder and affixed with parafilm (Figure 9.AB). Sterility was upheld by working with gloves in the sterile environment of a class 2 laminar air flow cabinet (LAFII) and double packing the holders in sterile Ziplock bags. Damage during transport in these bags was prevented by placement of 10 ml sterile test tubes over the tapered end of the holders. Holders were mounted in the reactor when a constant 37°C was maintained, the inoculum prepared and the experiment ready to begin. The holder placement was done by removing one of the stops of the lid and placing the holder in its opening, removing the 10 ml tube protecting the implants at the last moment. The holder was orientated such that its pin points to the centre, which was repeated for the second holder at the opposite side of the lid, in a 3 and 9 hour orientation with the outlet as reference at the 12h position (Figure 9.CD). Excess fluid was again collected and an additional 10ml was removed to account for the later added inoculum.

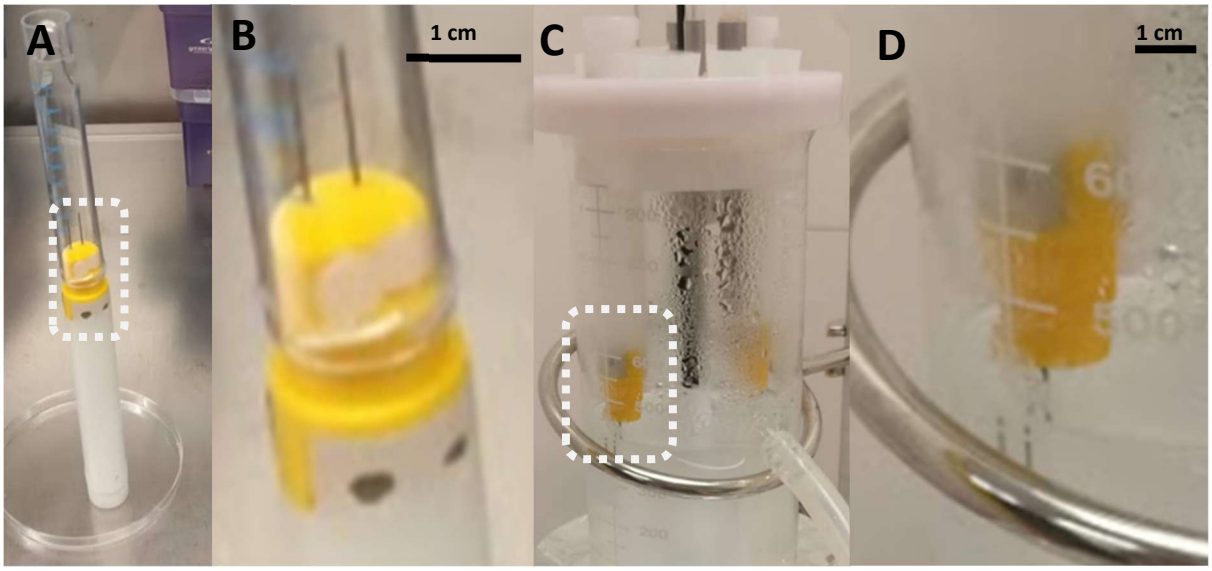

Figure 9. Steps of implant mounting. (A) Placement in sample holder. (B) Magnification of implant in sample holder. (C) Placement in reactor. (D) Magnification of implant in the reactor.

2.6.3 Dynamic adherence

Bacterial adherence in dynamic conditions was evaluated for the biofunctionalized implants (n = 4 per group, 1 group per run, all performed in duplicate) using the custom bioreactor setup in which the 10 mm implant was exposed to the bacterial and dynamic conditions. Dynamic incubation took place in 400 ml PBS supplemented with 2.5 mg/ml D-Glucose inoculated to reach ± 7.5 x 10^6 CFU/ml based on the stock concentration. After 20h of rotation at 125 rpm and 37°C, the implants were retrieved for post processing.

2.6.4 Static adherence

To study the bacterial adherence on the implants (n = 4 per group simultaneously performed) in static conditions, 10 mm sterile implants were placed in individual wells of a 24-wells plate and incubated without dynamic disturbance for 20h in a humid environment at 37°C (Figure 10). The wells were inoculated with 1 ml of ± 7.5 x 106 CFU/ml each submerging the implants, prepared by diluting the bacterial stock used for dynamic adherence in a 1:400 relation in PBS supplemented with 2.5 mg/ml D-Glucose. During all bacterial activities, the implants are exclusively handled with tweezers that were cleaned in 70% ethanol and subsequently allowed to air-dry.

Figure 10. Static bacterial adherence in 24 wells plate (n = 4 implants per group).

2.6.5 Inhibition of bacterial growth and antibacterial effect

Antibacterial effect of the implants was qualitatively determined by a zone of inhibition (ZOI) assay. Blood agar plates (Colombia III 5% sheep blood, Becton Dickinson, Franklin Lakes, USA) were inoculated by swabbing the entire plate in three directions with a swab drenched ± 3 x 10^8 CFU/ml inoculum and subsequently allowed to dry for 15 min in a LAF2 cabinet. The 10 mm cut implants (n = 1 per group per plate, performed in duplicate) were then placed on the agar plate in their distinct regions. The zones of inhibition were quantified with ImageJ 1.53a (National Institutes of Health, USA), after 20h incubation in a humid environment at 37°C.

2.7 Microbiological assay and sample post processing

2.7.1 Viable bacteria in the media

Bacteria in the media were measured after inoculation (t0) and at the end of incubation (t20) for both adherence experiments. In the case of the dynamic experiment 1 ml aliquots were taken from the reactor media, for the static adherence these aliquots were instead 100 µl in size and collected from the inoculum (at t0) and from the well after incubation (t20). Bacteria content was counted after 20h incubation in humid environment at 37°C. CFU experiments were performed in duplicate. Original aliquots were stored at 4°C to allow repetition of measurements at different dilutions, these would be performed where initial measurement was inadequate.

2.7.2 Implant post processing for adherent bacteria

After incubation, the implants were aseptically removed from their respective experiment, rinsed by two pipet spouts of 1 ml PBS covering the entire surface and stored in 1.5 ml Eppendorf tubes containing 1 ml PBS for up to 5 days at 4°C. All implants were vortexed thrice for 5 seconds in new Eppendorf tubes containing 1 ml fresh PBS at speed “3” of a VWR Standard Heavy-Duty Vortex Mixer (VWR International, Pennsylvania, USA). After they were vortexed, some implants (n = 1 per group per run) were stored in 1 ml fresh PBS at 4°C, the other (n = 3 per group per run) were sonicated using a Branson Sonifier 250 (Branson Ultrasonics, Connecticut, USA) with output set to “3” and duty cycle at “50%”, samples were orientated such that the end of the sonication rod ended 2 mm under the fluid surface (Figure 11). Subsequently the number of adherent CFU was measured for the sonicated implants by plating 100 µl aliquots on blood agar plates in duplicate and quantifying the number of CFU after 20h incubation in a humid environment at 37°C. The implants were placed in fresh PBS, these and the sonicated tubes were stored at 4°C.

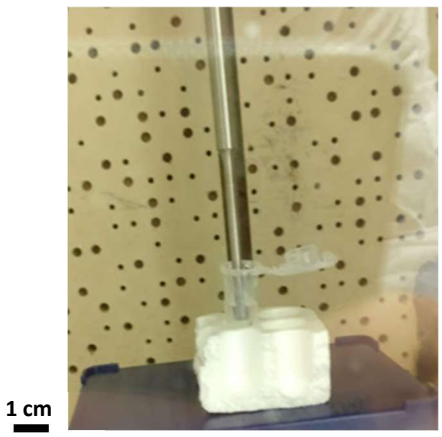

Figure 11. The sonication setup

2.8 Adherent bacteria visualization

Bacteria adhering on the implants stored in PBS at 4°C before and after sonication (n = 1 per group per experiment) were analysed by SEM. Implants were prepared by two 5 min cleaning steps in

demineralized water, followed by gradual dehydration by drenching the implants in 50% ethanol for 15 min, 70% ethanol for 20 min, 96% ethanol for 20 min and a 30 min douse in Hexamethyldisalazane (HMDS) after which the implants were dried in air for 2h. The implants were then ready for SEM imaging, performed in similar fashion to the morphologic characterization executed after implant production. Images were scoured for signs of adherent bacteria, capturing imagines at different magnifications. For the sonicated group, the "1" implant of each run was stored in PBS at 4°C and later collected for dehydration.

2.9 Statistical analysis

Data of samples was expressed as mean ± standard deviation where applicable. To compare results these were exposed to a One-Way ANOVA followed by Bonferroni post-hoc to test statistical difference between the groups using Microsoft Excel (Office 365) assisted by the Analysis Toolpak add-in. Differences were considered statistically significant at $p < 0.05$.

Chapter 3 Results

3.1 PEO surface biofunctionalization process

The voltage over time was monitored during the PEO process and collected for the PEO, PEO + 0.3 g/l AgNPs, and PEO + 3.0 g/l AgNPs implants (Figure 12). For the first 8 ± 0.5 seconds a linear increase of voltage is recorded reaching 116 (± 2.61) V, at 13.25 (±0.46) V/s. At this point the applied voltage exceeded the breakdown voltage for the implants causing the oxide layer to become electrically conductive leading to the so-called dielectric breakdown process. After this change in conductivity of the oxide layer, the plasma discharges are initiated recognised them by formation of sparks (Figure 13.AB), as well as accompanied by a crackling sound. In this phase the graph follows a smooth gradual increase of voltage over time, reaching a final voltage of 244.5 ± 7.9 V after 300 s of PEO. Similar characteristics were seen for the different implants, but the voltages reached were slightly lower for the AgNPs incorporated procedures.

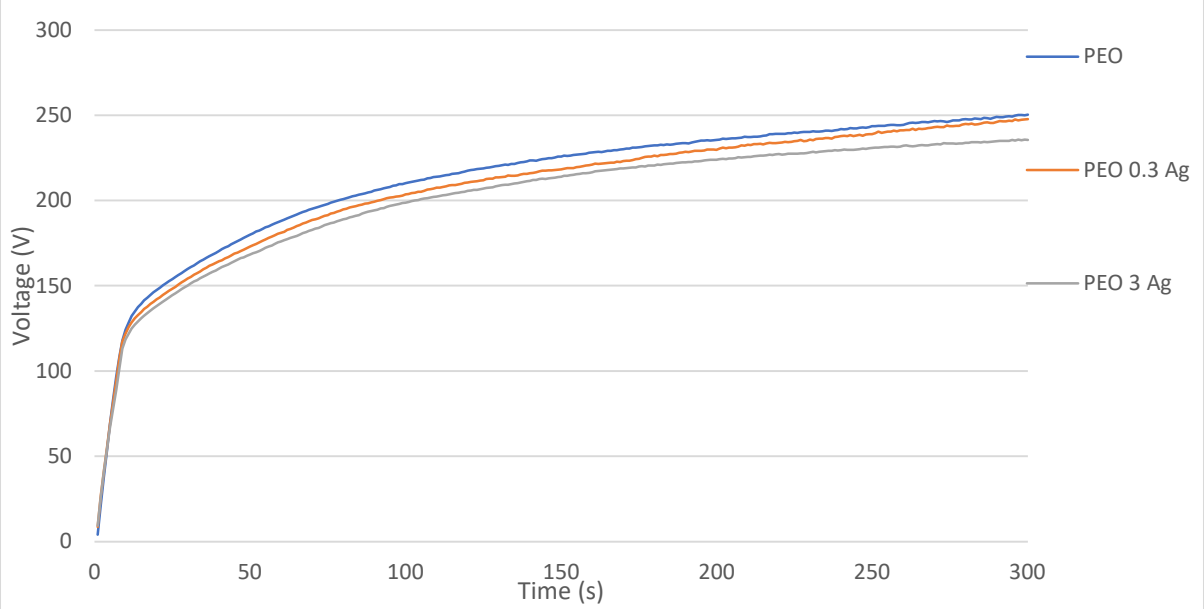

Figure 12. Voltage – time data recorded during PEO process for different Ti6Al4V implants.

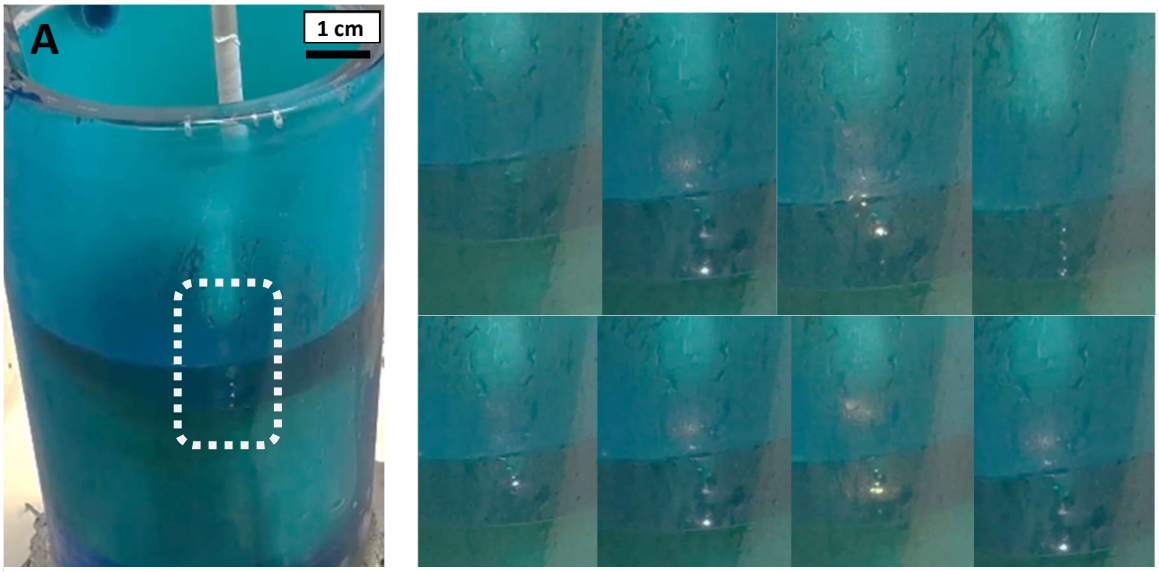

Figure 13. Spark discharge during PEO process without silver after dielectric breakdown. (A) PEO electrolytic cell with zone of interest on mounted implant. (B) Close view of this zone of interest during the process.

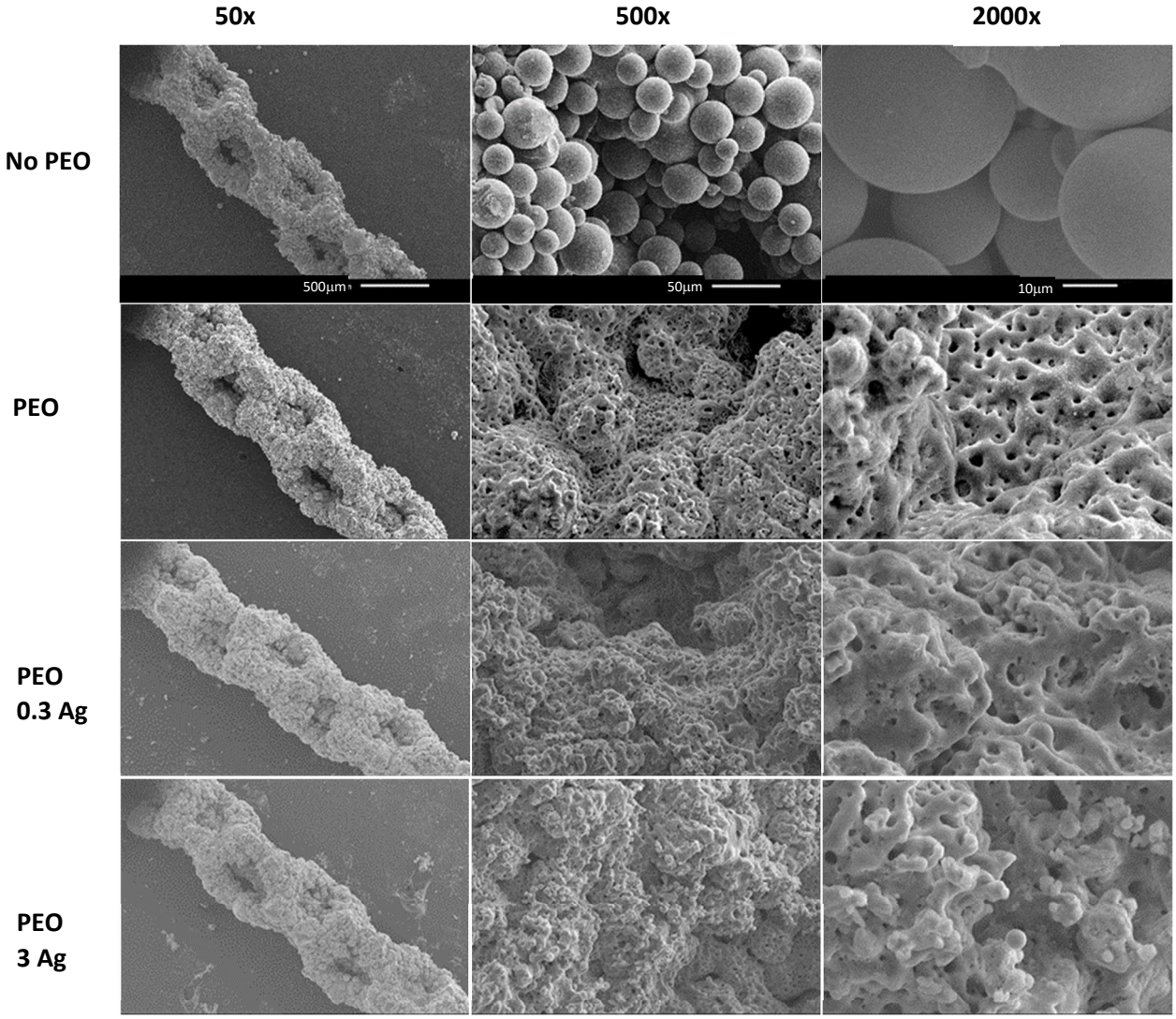

Figure 14. SEM imaging of the implants at 50-, 500- and 2000- times magnifications, in untreated (No PEO) state and after undergoing PEO with no, 0.3 g/l and 3 g/l AgNPs, respectively.

3.2 Morphologic and chemical analysis

3.2.1 Implant surface morphology

The implant surface morphology was analysed by SEM at different magnifications (50x, 500x and 2000x) for the 4 implant groups (Figure 14). Clear differences are seen between the non-PEO treated and PEO-treated groups while no significant differences are observed within the PEO treated groups.

3.2.2 Surface layer elemental composition

The presence of AgNPs incorporated on the implant oxide layer following the PEO treatment was confirmed by EDS analysis and displayed in Figure 15. As can be observed from EDS spectrat, the following elements were identified: Ag, C, Ti, O, Al, P and Ca. Among these the Ag, P and Ca are additives corresponding to the electrolyte contents which were incorporated in the oxidized layer, while the Ti and Al were part of the implant alloying elements. No such Ag peaks were observed for any of the other analysis sites, where only a spread of the soluble Ca and P, together with the implant alloying elements (i.e. Ti and Al) were found.

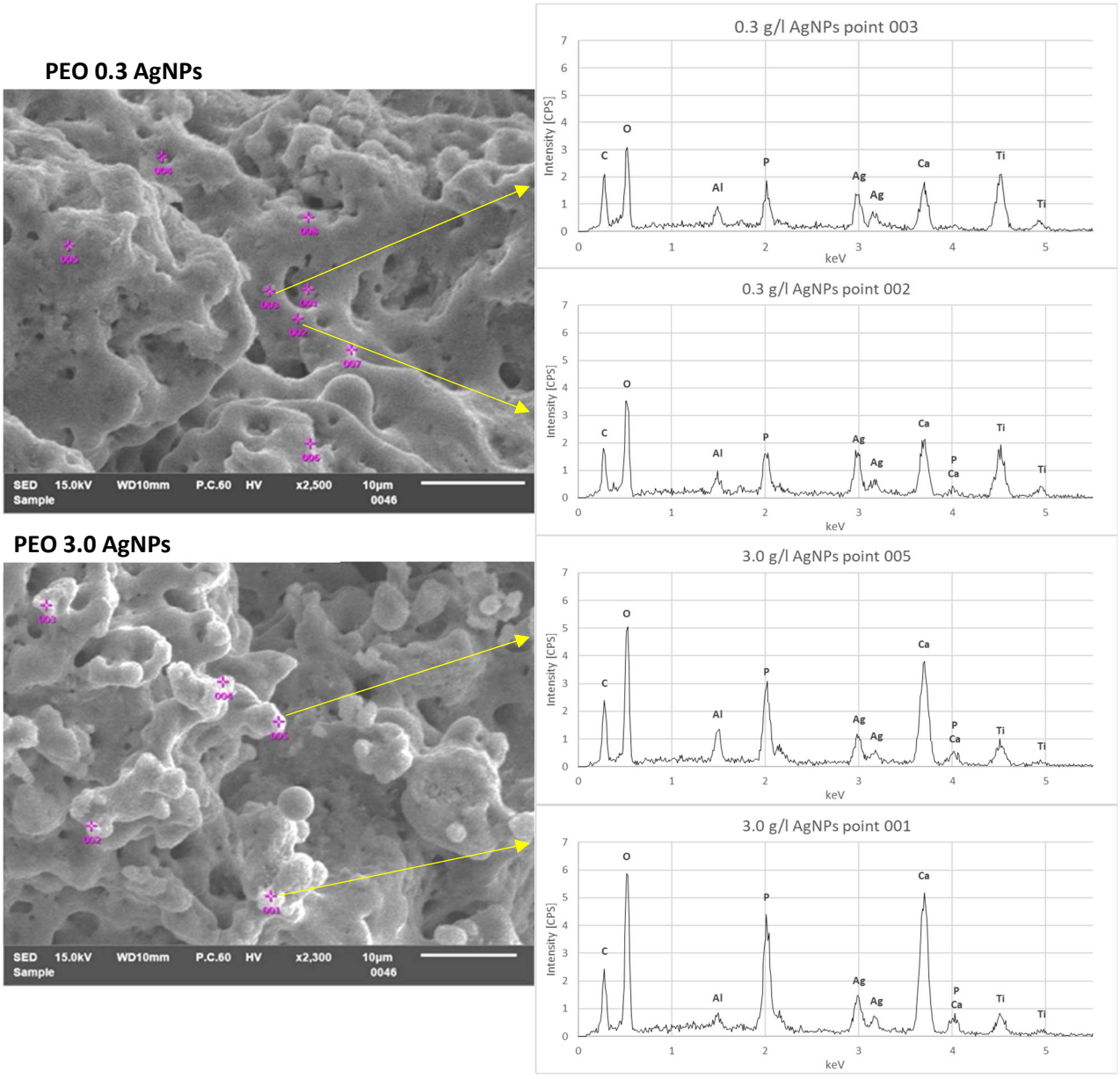

Figure 15. EDS point analysis on the 0.3 g/l and 3.0 g/l AgNPs PEO implants indicating the presence of incorporated AgNPs as well as the oxide layer chemical composition.

3.2.3 Release of Ag ions

The release of Ag ions (Ag^+) from the silver nano particles incorporated on the implant surface was measured over a 24 h period at 4 time points, such as 3, 6, 12 and 24 h, and presented in Figure 16. For the 3.0 g/l AgNPs implants a higher release of silver ions is seen in the cumulative release profile. Both groups are continuously releasing more silver ions. For the 3.0 g/l AgNPs implants this release is gradually decreasing, while for the 0.3 g/l AgNPs implant silver ion release appears to be more or less constant during this 24h period.

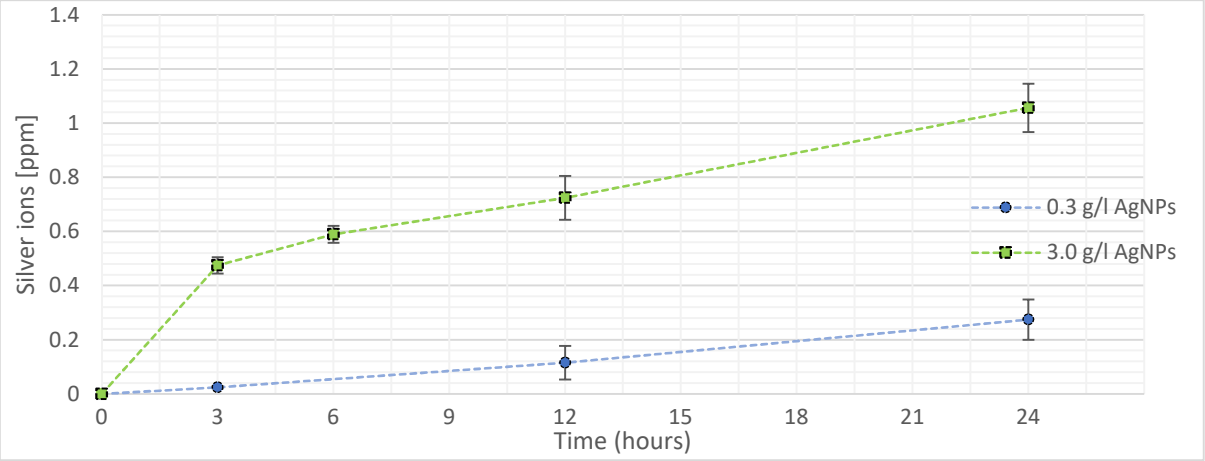

Figure 16. Cumulative Ag^+ release profile for 0.3 g/l PEO and 3 g/l PEO treated implants (n = 3).

3.3 Inhibited bacterial growth around implants

Implants with AgNPs incorporated exhibited zones of inhibition only for the implants with the 3.0 g/l concentration group. No inhibition of growth was observed for the implants without silver, while the 0.3 g/l AgNPs incorporation only displayed the zone of inhibition in the close perimeter of direct contact with the agar. ZOI's measured for the 0.3 g/l (Figure 17.C) and 3.0 g/l (Figure 17.D) groups are 9.6 (±0.4) mm^2 and 17 (± 0.8) mm^2 respectively.

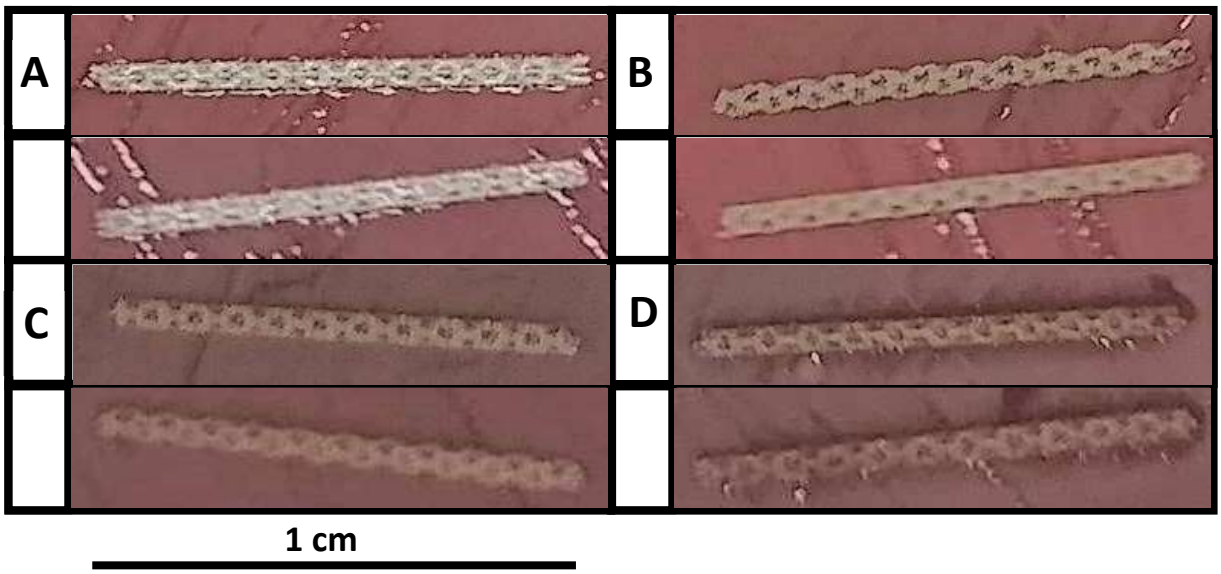

Figure 17.The ZOI of Ti6Al4V implants: (A) No-PEO, (B) PEO treated, (C) PEO with 0.3 g/l and (D) PEO with 3.0 g/l AgNPs. Implants are 10 mm in length.

3.4 Bioreactor setup

3.4.1 Implant holder

The modular insert (Figure 18.B) was designed with SOLIDWORKS 3D (Dassault Systémes, Paris, France) to fit a machined original holder (Figure 18.A). Functional prototypes (Figure 18.C) were manufactured in PLA filament using a desktop 3D printer, the holes holding the implants were drilled in post-processing.

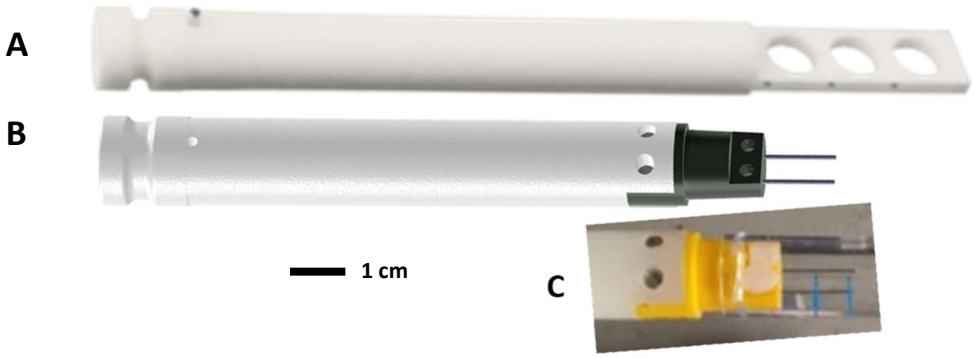

Figure 18. Sample holder rods for the CDC bioreactor. (A) Original sample holder. (B) Modified version with modular insert (black). (C) Insert (yellow) as produced in use.

3.4.2 Method adjustments

To achieve bacterial adherence the custom bioreactor setup was experimentally optimized. A range of test runs was performed with their results considered for the experiments performed thereafter. For the range of 12 trials the initial and final bacterial media concentrations were collected (Figure 19), to provide context some trials had additional outcomes such as control of temperature and count of viable bacteria swabbed from the samples or the reactor vessel (Table 4). As for some trials the media content was also analysed on additional time points, these were collected and presented together with the initial and final concentrations (Figure 19). Among these trials it was seen that final bacterial concentration in the media occasionally showed no remaining viable bacteria (consistently seen for T3, T4, and T6). For the follow ups where bacteria content was measured at multiple time points both reduction (T7, T9, T10 & T12) and loss of bacteria (T8 & T11) was measured.

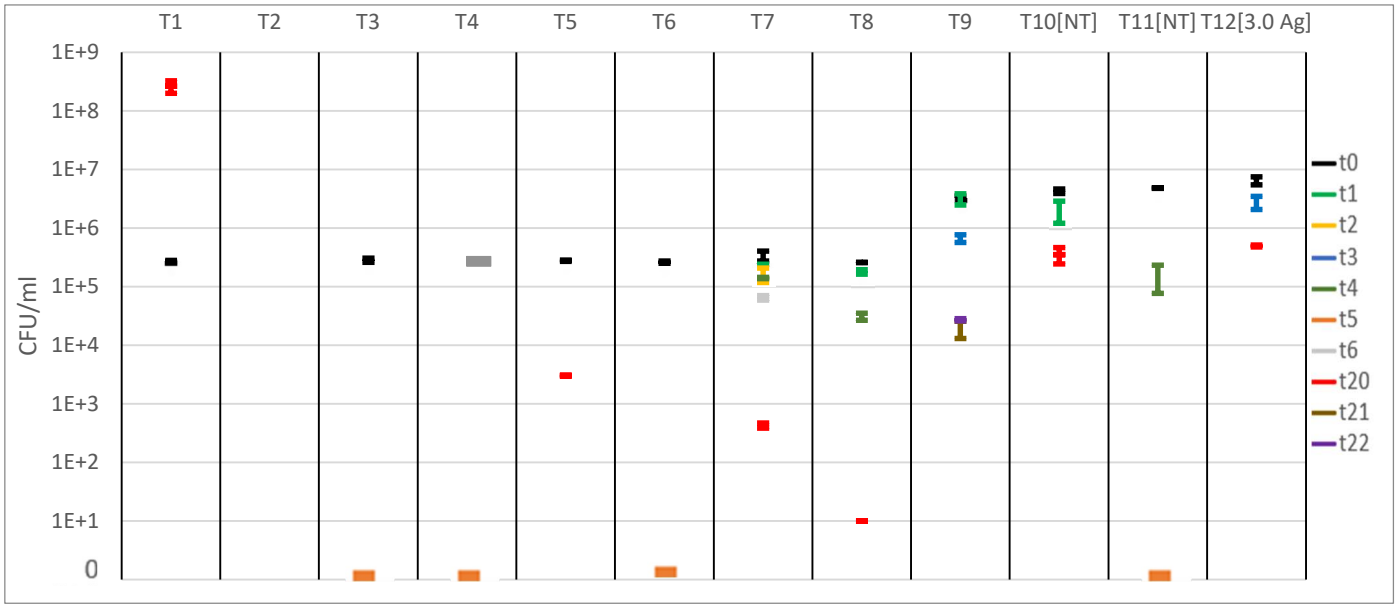

Figure 19. Media concentrations of the dynamic adherence trials T1 – T12. Measured in duplicate, at t = 0 and 20 h, with additional measurements at 1 – 6, 21 or 22 h for T7 – T12.

Table 4. Additional results for dynamic adherence trials T1 – T12. Bacterial content in media (t20) (seen in Figure 19) is presented in the first column, experimental results are provided in the second column. Setup described in Table 2.

T1 ***2.7(±0.5)*** ***x10^{8} CFU/ml***	Media at t20 → **Turbid** Samples (***Ti-6Al-4V discs***) swabbed at t20→ **1.8 x 10^{2} CFU**
T2	Blank run
T3 ***0 CFU/ml***	Samples (*Ti-6Al-4V discs*) swabbed at t20 → **0 CFU**
T4 ***0 CFU/ml***	Samples (*Ti-6Al-4V discs*) swabbed at t20 → **0 CFU** Shake incubator duplicate; Bacteria at *t0:* **3.8 x 10^{5} CFU/ml;** *t20:* **1.1 x 10^{4} CFU/ml** Compared to **2.7 x 10^{5} CFU/ml** and **0 CFU/ml** for the reactor run
T5, ***3.1(± 0.6)*** ***x10^{3} CFU/ml***	Samples (*Ti-6Al-4V discs)* swabbed at t20→ **2.9 x 10^{2} CFU** Samples (*Ti-6Al-4V discs + implants)* post-adherence, incubated in TSB o/n at 37°C → **Turbid** Reactor wall swab → **6.1 x 10^{2} CFU** Reactor outlet swab → **8.6 x 10^{2} CFU** Temperature during the experiment → **38-40 °C** measured on the reactor wall.
T6 ***0 CFU/ml***	Samples (*Ti-6Al-4V discs)* swabbed at t20→ 0 **CFU** Samples (*Ti-6Al-4V discs + implants)* post-adherence, incubated in TSB o/n at 37°C → **Clear** Reactor wall swab → **0 CFU** Reactor outlet swab → **0 CFU** Temperature during the experiment → **39-42 °C** measured on the reactor wall.
T7 ***4.3(±0.3)*** ***x10^{2} CFU/ml***	Reactor wall swab → **6 x 10^{1} CFU** Reactor outlet swab → **8 x 10^{1} CFU** Temperature during the experiment → **38(± 0.5) °C** measured on the reactor wall.
T8 ***1*** ***x10^{1} CFU/ml***	Reactor wall swab → **0 CFU** Reactor outlet swab → **0 CFU** Temperature during the experiment → **36-38 °C** measured on the reactor wall.
T9 [t22] ***2.7(±0.09)*** ***x10^{4} CFU/ml***	Reactor wall swab → **1.48 x 10^{3} CFU** Reactor outlet swab → **1.84 x 10^{3} CFU**
T10 ***3.6(±0.8)*** ***x10^{5} CFU/ml***	Reactor wall swab → **6.7 x 10^{4} CFU** Reactor outlet swab → **5.7 x 10^{4} CFU** Bacteria on samples (Ti-6Al-4V implants) [no pre-cleaning, 5 min son.] → **Fully covered agar plate at -1 log**
T11 ***0 CFU/ml***	Reactor wall swab → **6 x 10^{1} CFU** Reactor outlet swab → **9 x 10^{2} CFU** Bacteria in media after *shared* 5x 10s vortex pre-cleaning → **1.78 x 10^{4} CFU/ml** **Adherent** bact. on individual samples (Ti-6Al-4V implants) [5x 10s vor. pre-cleaning, 5 min son.] → **6.9 x 10^{3} CFU/ml, 8.6 x 10^{3} CFU/ml & 4.2 x 10^{3} CFU/ml.** Average; **6.6(± 2.2) x 10^{3} CFU/ml**
T12 ***4.9(±0.1)*** ***x10^{5} CFU/ml***	Bacteria in media after *individual* 3x 10s vortex pre-cleaning → **1.6 x 10^{3} CFU/ml** **Adherent** bact. on individual samples (Ti-6Al-4V implants) [3x 10s vor. pre-cleaning, 3 min son.] → **1.0 x 10^{4} CFU/ml & 5.3 x 10^{3} CFU/ml.** Average; **7.7(± 3.4) x 10^{3} CFU/ml**

3.5 Shear simulation

Shear rate in the reactor was simulated for the rotation of the stir blade at 45° increments of the stir blade (Figure 20), the implant position in relation to these angle increments correspond to Figure 7 B. From these simulated shear rates the associated shear stresses were calculated (Table 5) in 2 mm increments along the implant length from the fluid surface to its 10 mm depth in the media at both holders (A&B side). Within the shear stresses the highest difference (SD: 1.9 x 10^{-2} mPa) was found at the 0° position of the stir blade at the media surface level, peak shear stress for a given location varies

for different stir blade positions while being consistent for both the A and B implant locations as labelled in Figure 7B. The average shear stress found on the implants for these orientations was 0.58 (± 0.029) mPa.

Table 5. Shear stress in mPa along the implant depth in the media for both holders during the rotation, at 45° increments for A and B side of the reactor

	Shear stress [mPa]															
Subsurf.		**0°**				**45°**				**90°**				**135°**		
[mm]	A	B	mean	sd	A	B	mean	sd	A	B	mean	sd	A	B	mean	sd
0	0.55	0.58	0.56	2E-02	0.58	0.58	0.58	8E-04	0.61	0.61	0.61	2E-04	0.57	0.56	0.57	8E-03
-2	0.55	0.57	0.56	1E-02	0.59	0.59	0.59	3E-04	0.61	0.61	0.61	4E-04	0.57	0.56	0.56	5E-03
-4	0.54	0.55	0.55	5E-03	0.59	0.59	0.59	5E-04	0.61	0.61	0.61	3E-03	0.56	0.55	0.56	2E-03
-6	0.53	0.54	0.53	3E-03	0.59	0.59	0.59	8E-04	0.62	0.62	0.62	7E-04	0.55	0.55	0.55	8E-04
-8	0.53	0.54	0.53	3E-03	0.60	0.60	0.60	1E-03	0.61	0.61	0.61	8E-04	0.55	0.55	0.55	1E-03
-10	0.53	0.54	0.53	7E-03	0.61	0.61	0.61	1E-03	0.60	0.61	0.61	3E-03	0.55	0.55	0.55	4E-04

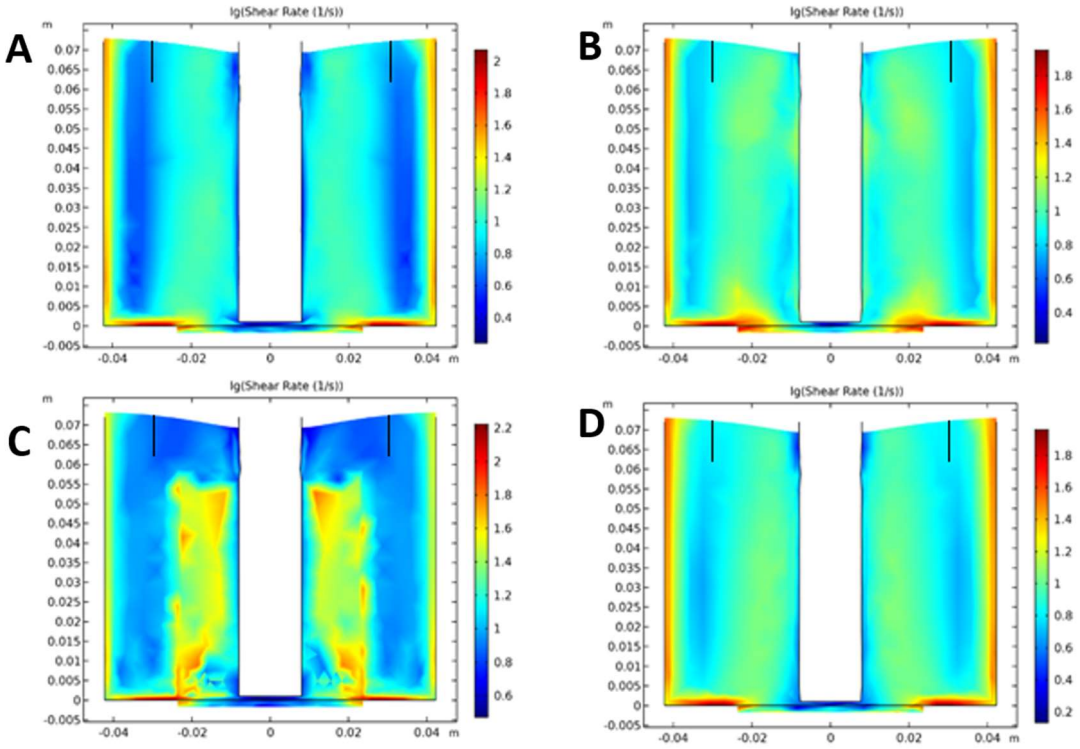

Figure 20. Shear rates during simulation of 125 rpm, for 4 different stir blade orientations at (A) 0°, (B) 45°, (C) 90° and (D) 135°.

3.6 Bacterial adherence qualitative measurements

Both dynamic and static adherence experiments had their concentrations measured at the start of the experiment after incubation (t0) and at the end (t20) of the experiment. These measurements served as control with for t0 averages at 1.6(±1.3) x 10^7 CFU/ml for the dynamic (Figure 21), and 5.1 x 10^7 CFU/ml for the static assays (Figure 23). In the dynamic experiments 4 out of 10 of the experiments had zero measurements for the bacteria in the media at t20, where for the trials this was comparably the case for 1 of the 4 experiments with adjusted inoculum (T9 onwards) (Figure 19). The bacterial adherence on the implants which was measured for dynamic (Figure 22) and static (Figure 24) experiments shows consistent levels of adherent bacteria on the n = 3 implants within the runs with non-zero bacteria content at t20 (D1, D3, D5), average adherence for these runs were 3.00(±0.43) x 10^4 CFU/ml, 1.88(±0.45) x 10^4 CFU/ml and 9.13(±2.42) x 10^3 CFU/ml respectively with a significant difference ($p < 0.05$) between D1(NT) and D5(0.3Ag) groups. Some of the runs in this dynamic experiment did show adherent bacteria recovered from three (D4, PEO) or two (D7, 3.0Ag) of the

three implants without bacteria measured in the media at t20. For the static experiment a decrease of t20 concentration was measured for the different groups with significant difference ($p < 0.05$) between the T2(PEO) – T3(0.3Ag), T2(PEO) –T4 (3.0Ag) and the T3(0.3Ag) – T4 (3.0Ag) groups. Similarly, a significant difference was seen in the decrease of adhering bacteria measured for the static experiments between S1(NT)-S3(0.3Ag) ($p < 0.05$) while for the S1(NT)-S4(3.0Ag), S2(PEO)-S3(0.3Ag) and S2(PEO)-S4(3.0Ag) a higher level difference was found ($p < 0.001$).

3.7 Visualization of adhering bacteria

Adherent or remnant bacteria were observed on the implants after the experiment (Exp.) and after removal of bacteria by sonication (Son.) (n = 1 per run) for the adherence assays. Implant surface was explored for the Staphylococcus reminiscent orbs, SEM images collected at 2000-times magnifications were compared for qualitative analysis (Figure 25). A visual spread of adhering bacteria is seen on the Exp implants of the static experiment regardless of silver content with lesser visual adherence on the smooth NT samples (Figure 25.A, Exp), no bacteria were visible on the surface after sonication (Figure 25.A, Son). For the dynamic assay adherence is seen for the analysed NT, PEO and 0.3Ag implants (Figure 25.B, Exp), for the NT and PEO implants this hints at biofilm formation while the 0.3Ag group only had adherence occurring in the cavities. After sonication (Figure 25.B, Son) a spread of bacteria on the implant surface was observed for all these groups.

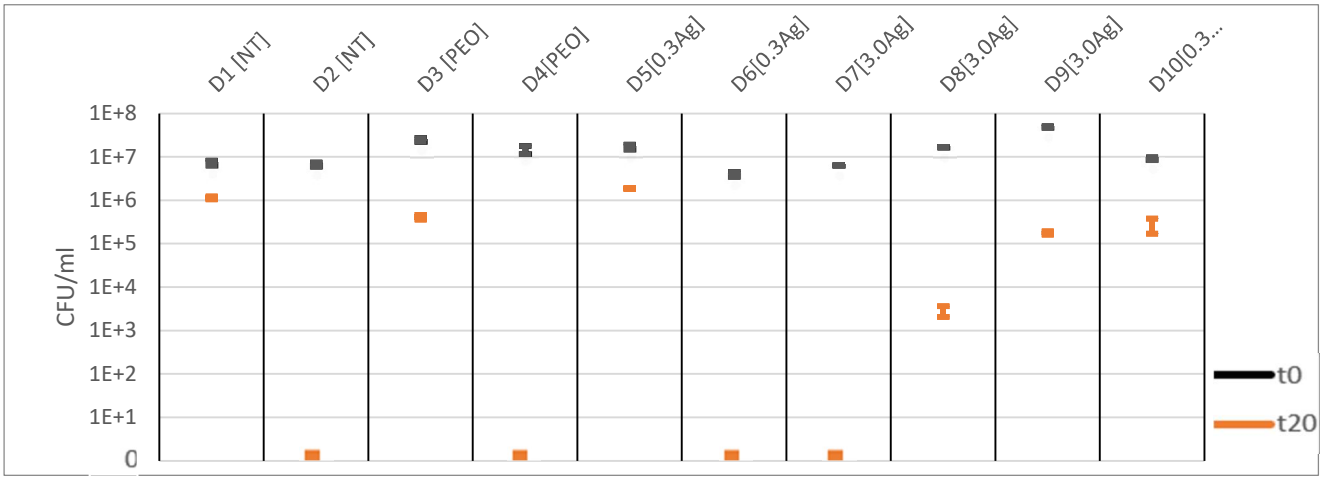

Figure 21. Bacterial concentration in the media of the dynamic adherence assay, measured in duplicate, at t = 0 and 20 h.

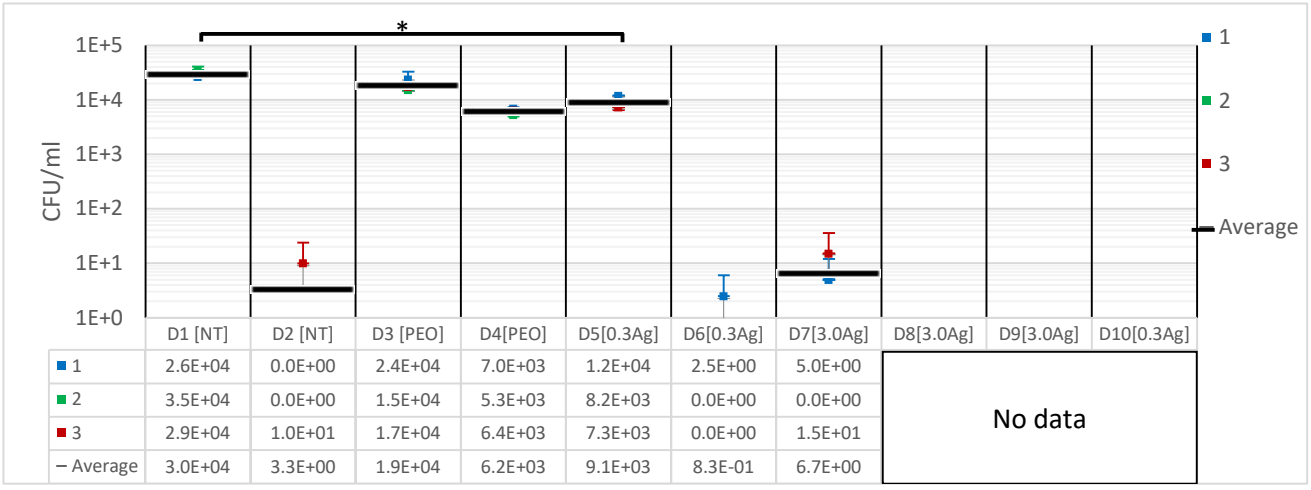

	D1 [NT]	D2 [NT]	D3 [PEO]	D4[PEO]	D5[0.3Ag]	D6[0.3Ag]	D7[3.0Ag]	D8[3.0Ag]	D9[3.0Ag]	D10[0.3Ag]
1	2.6E+04	0.0E+00	2.4E+04	7.0E+03	1.2E+04	2.5E+00	5.0E+00			
2	3.5E+04	0.0E+00	1.5E+04	5.3E+03	8.2E+03	0.0E+00	0.0E+00			
3	2.9E+04	1.0E+01	1.7E+04	6.4E+03	7.3E+03	0.0E+00	1.5E+01			
– Average	3.0E+04	3.3E+00	1.9E+04	6.2E+03	9.1E+03	8.3E-01	6.7E+00			

Figure 22. Dynamic experiment. Adherent bacteria, n = 3 implants per run (marked as 1, 2 and 3), 2 runs per implant group (D1-D8), with D9-D10 as repeat of D7 and D6 respectively. Average per group plotted with SD bar. Runs with non-zero bacteria content at t20 (D1, D3 & D5) were tested with Bonferroni-post hoc where D1-D5 was significantly different (*, $p > 0.05$).

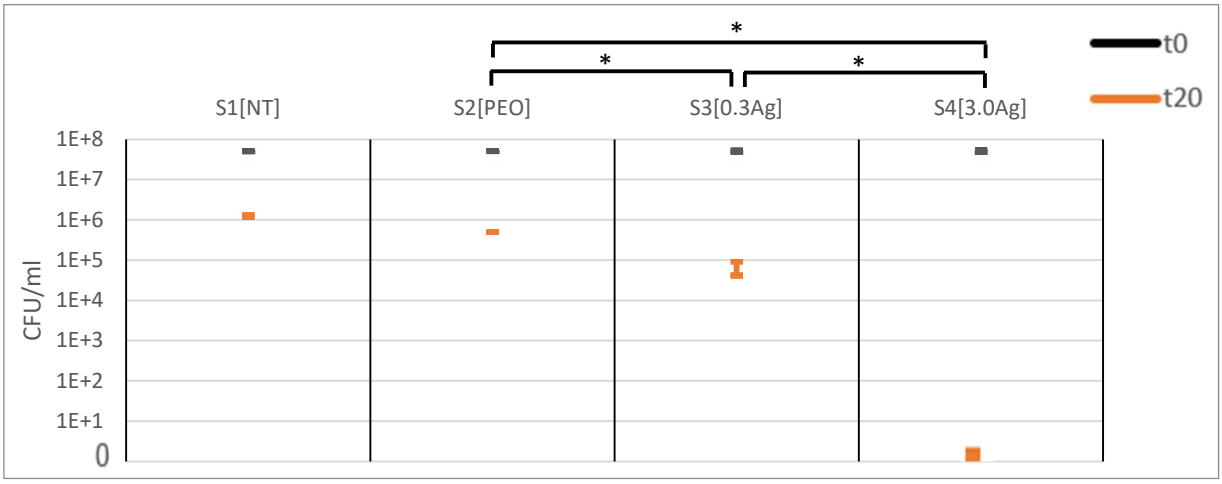

Figure 23. Bacterial concentration in the media of the static adherence assay, measured in duplicate, at t = 0 and 20 h. Bacterial concentration at t20 tested with Bonferroni-post hoc, significant differences found for S2-S3, S2-S4 and S3-S4 (*, p < 0.05)

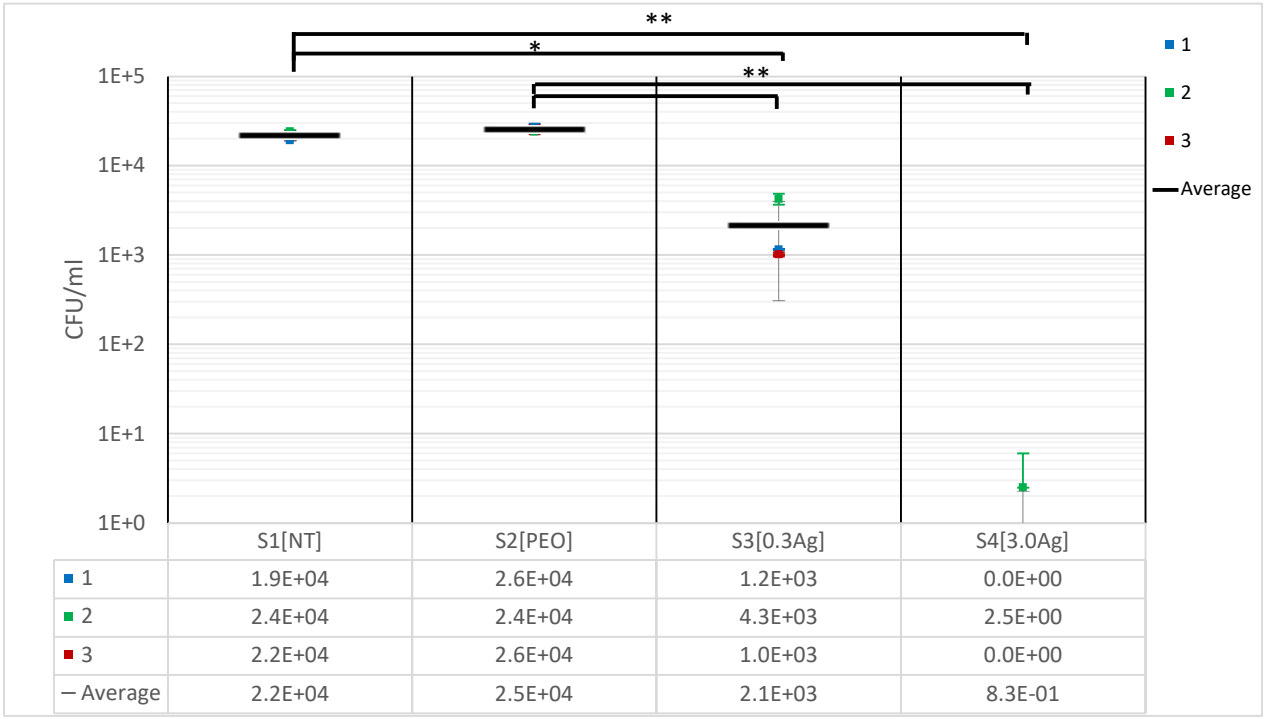

	S1[NT]	S2[PEO]	S3[0.3Ag]	S4[3.0Ag]
1	1.9E+04	2.6E+04	1.2E+03	0.0E+00
2	2.4E+04	2.4E+04	4.3E+03	2.5E+00
3	2.2E+04	2.6E+04	1.0E+03	0.0E+00
Average	2.2E+04	2.5E+04	2.1E+03	8.3E-01

Figure 24. Static experiment, Adherent bacteria, n = 3 implants per run (1, 2, 3), 2 runs per implant group (S1-S4), with D9-D10 as repeat of D8 and D6 respectively. Average per group plotted with SD bars. Differences in bacterial adherence were significant for S1(NT) – S3(PEO) (*, p < 0.05), with differences between S1(NT)-S4(3.0Ag), S2(PEO)-S3(0.3Ag) and S2(PEO)-S4(3.0Ag) being more significant (, p < 0.001). Significance was tested with Bonferroni-post hoc.**

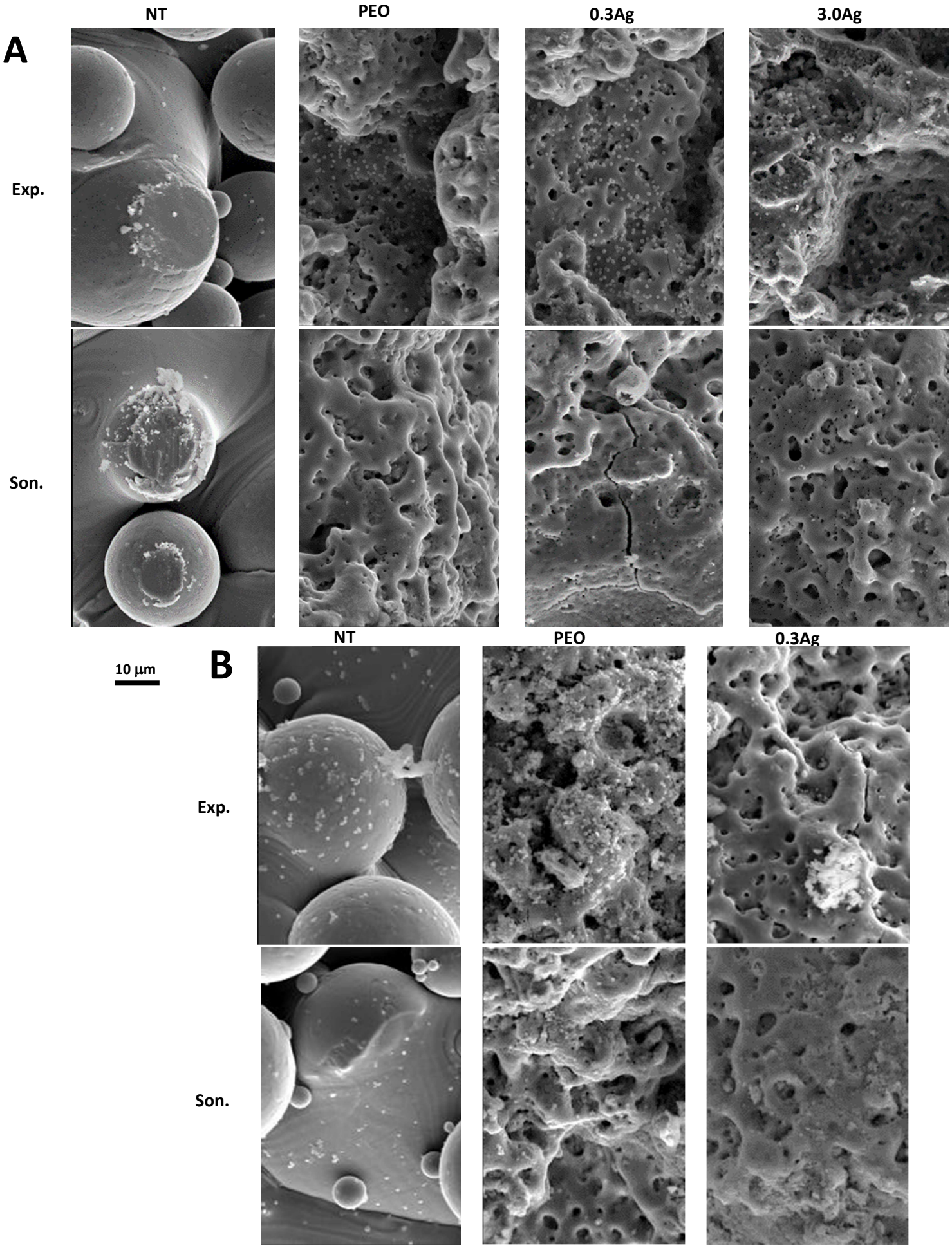

Figure 25. SEM images of implants after incubation (Exp.) and after (Son.) removal of non-adherent bacteria, at 2000-times magnifications for static (A) and dynamic (B) experiments with the NT, PEO, 0.3Ag and 3.0Ag groups respectively

Chapter 4 Discussion

4.1 Implant characterization

In this study, the 3D printed Ti6Al4V implants, with and without addition of AgNPs by PEO process, were characterized with respect to their oxide surface morphology, surface chemistry, silver ion release, and antibacterial effect (both static and dynamic conditions). The primary outcomes of implant synthesis, such as the morphology of V-t curves, the values of the dielectric breakdown voltage, and the maximum voltage, seemed to be in line with the previous findings [20-22]. In this study, the dielectric breakdown of the 3D printed Ti6Al4V implants was obtained at 116 ± 2.61 V after 8 ± 0.5 sec while the maximum voltage was found at 244.5 ± 7.9 V. In the previous studies [20-22], the V-t graphs had similar form while the breakdown and maximum voltages were at 115±5V//245±5V and 115±5V//249±6V, respectively.

Morphological changes and surface chemistry after PEO were analysed for the different implant groups and compared with the previous studies [20-22]. As-manufactured implants (NT) had distinctive macro porous structure with spherical and relatively smooth Ti-6Al-4V powder of ± 20-50 μm bonded to its geometry in partially melted and un-melted state, an inherent SLM attributed characteristic [43]. The high voltage sparks induced during PEO have changed the smooth implant surface to a uniform microporous oxide layer, with no quantifiable differences between the PEO, 0.3Ag and 3.0Ag implants. The formed layer does contain the Ca and P electrolytic species for each of the groups together with the implant alloying elements detected by the EDS method. The chemical composition of the oxide layers was consistent with those of previous work, with the same elemental peaks despite lower counts per second or missing vanadium peak at the 4.9 KeV, which was an SEM machine-related issues [44].

The silver content in the electrolyte was 0.3 g/l and 3.0 g/l AgNPs for 0.3Ag and 3.0Ag. The release of silver ions in PBS was measured at 4 time points over a 24h period, a length comparable to the 20h adherence experiments. For the 0.3Ag and 3.0Ag a cumulative release of 0.27 (± 0.07) and 1.06 (± 0.09) ppm was measured at 24h. The release of silver ions for 3.0 g/l electrolyte concentration had previously been measured to be 0.9 (±0.1) ppm was found making the implants' silver release comparable [20, 21]. The different relationship between the ion release and electrolyte contents is an expected effect, as the silver NPs are not solely incorporated on the outer surface but are also in enclosed cavities (micropores) developed during the process of PEO.

Silver NPs were incorporated on the implant surface to favour its antibacterial effect. This has been observed by the formation of a ZOI around the implant. The ZOI of 3.0Ag implants had a larger area than the 0.3Ag group, where this occurred mostly underneath the implant (Figure 17.C). Previous antibacterial analysis with ZOI assays displayed more prevalent inhibition 2 to 3 times as wide [20, 21]. As these utilised 15 mm cut implants, 10^7 CFU/ml swabs and MRSA strain USA300, compared to the 10 mm cut implants, 10^8 CFU/ml swabs and *S. aureus* strain 35556 which were utilised in this study this difference is not unexpected. For previous studies the minimum bactericidal concentration (MBC) and minimum inhibitory concentration (MIC) of silver were determined for the MRSA USA300 strain as 60 μM and 4 μM respectively, determining these for the SA 35556 would give context to whether the differences are strain, or methodology based [20]. Despite lacking absolute similarity between this and previous studies, the 3.0Ag and 0.3Ag both showed antibacterial properties which, for this study, validates their antibacterial effect.

4.2 Bioreactor model and method of adherence

Novel biomaterials are in development to hinder the occurrence of implant related infections. For these materials positive antibacterial effect seen in static experiments might differ in dynamic

conditions experienced *in vivo*, which this study analysed for prevention of bacterial adherence on (silver incorporated) PEO treated implants in development at TU Delft. Prevention of adherence was the specific goal, as adherence results in implant colonization, biofilm growth, prevention of bone attachment and severe short- or long-term septic implant loosening and infections [17, 18].

Dynamic conditions were applied on the implants mounted in custom holders, in which the 2 cm long (∅0.5 mm) implant cuts were mounted with 10 mm of these in the media. Two implants were mounted per holder, with the holders removable from the holder to be swapped for other sample holders. Current holders were 3D printed with PLA filament, instead of machining them from resilient, water-resistant lab-grade material due to time budget and limited number of runs (± 30). The implants were fixated by parafilm plugs instead of the designed mechanism due to the same pragmatic reasons.

Bioreactor dynamics and media content were altered to prevent bacterial multiplication that would hinder comparison between (antibacterial) materials, these customizations included low nutrient media and no nutrient-/waste transport [45, 46]. Experiments testing the bioreactor setting, preceded the dynamic experiments. Nutrient content was tested at 10% TSB (T1), which caused multiplication like stock solution, which was then adjusted to ± 0.1% TSB with 2.5 mg/ml glucose for follow up experiments. The first analysis' of this new media resulted in total loss of bacteria (T3,4), with an external shake incubator run parallel to T4 an accepted 1 log reduction was measured instead which implies that the media was sufficient and that loss of bacteria had a different cause. This could be disinfectant remnants of cleaning which had a continuous effect during the experiment, while the aliquot only had temporarily been exposed. To eliminate this, further cleaning included a thorough demineralized water rinse after chlorine disinfectant contact, alternatively temperature could also be the cause which was analysed by temperature logging. In addition, the adherence to implants and reactor walls was qualitatively analysed as adherence implied reduction of suspended bacteria.

Further experiments displayed normal temperatures within the 36-42°C limits, adherence on the reactor walls/implants, and 2 fold reduction of bacteria concentration was measured (Figure 23). Despite this occurring (T5), zero suspended bacteria were similarly found for others (T6). To further omit reasons for this loss of bacteria, the dynamics and bioreactor elements were stepwise re-introduced, keeping the previous alternations. In the first run hereafter the bacterial content in the media was measured at different time points while the stirring, stir mechanism, sample holders and samples were all omitted (T7). Despite the log 3 reduction of the bacteria, attributed to the settling of the bacteria by lack of flow, bacterial adherence was found, and the stirring was re-introduced in the next run (T8).

After once more having zero suspended bacteria in this run, the bacterial concentration was 10-fold increased to reach ± 3 x 10^6 CFU/ml in the media, which when applied for a repetition of T8 resulted in a positive 2 log reduction of bacteria (T9). Follow up experiments then step wise reintroduced the implants (NT in T10, 3.0Ag in T12), and aimed to optimise the removal of adherent bacteria to allow measurement of the number of adherent bacteria (T10-T12). With more consistent adherence due to the alterations, this was continued for the dynamic experiments performed hereafter.

Fluid shear experienced by the implants followed from the reactor dynamics simulated by computational fluid dynamics (CFD), which resulted in an average shear stress of 0.58 mPa = 0.0058 dynes/cm^2 at 125 rpm. Previous research utilising unadjusted CDC bioreactor models occasionally reported "high" shear forces due to the dynamics [28, 36, 47, 48]. To give context to the found shear stresses instead of labelling, they were compared to some know *in vivo* experienced shear forces. Some of the physiological shear stresses known *in vivo* are those within arteries, veins and interstitial fluid and are in the 10-70 dynes/cm^2, 1-6 dynes/cm^2 and 0.006-0.015 dynes/cm^2 ranges respectively

[49, 50]. Shear stresses experienced by the implants in the bioreactor simulation are within the range of *in vivo* shear stresses occurring due to interstitial fluid flow dynamics.

4.3 Bacterial adherence

Analysis of bacterial adherence for both static and dynamic conditions occurred by CFU count of bacteria removed from the implants after 20h incubation when bacteria were measured in the media at the point of implant removal. Despite following the adjusted procedure a pattern emerged where every other experiment until D7 encountered total loss of bacteria (D2(NT), D4(0.3Ag) and D6(3.0Ag)), their duplicates were however successful with ± log 2 reduction and had their implants subsequently analysed on adherence. Experiments with no bacteria measured were queued for repetition and excluded from further interpretation. With primary interest in the antibacterial capabilities priority was given to repetition of 0.3Ag (D10) and 3.0Ag (D09) over the non-silver containing groups, both repetitions had a successful ± log 2 reduction of bacteria. For static conditions a difference in log reduction is measured compared to the dynamic experiments, with increasing reduction from ± log 1 for the NT and PEO control groups to ± log 3 for the 0.3Ag and near zero bacteria left for 3.0Ag while this was a constant ± log 2 reduction for the dynamic experiments. This difference was within expectancy due to the dilution of ion's in the high volume of the reactor, as compared to the smaller static assay volume.

Bacterial adherence for the dynamic experiment was analysed for the available data (D1(NT), D3(PEO), D5(0.3Ag)), which misses the last three successful dynamic experiments (D8(3.0Ag), D9(3.0Ag) and D10(0.3Ag)) due to COVID-19 related lab closure. Which prohibited access to the hospital and its labs for all, non-highly essential microbiology department personnel. Data which had been gathered prior displayed a comparable adherence between the NT and PEO groups of the dynamic experiment, as expected for non-silver groups. The 0.3Ag group had a $p < 0.05$ significant log 0.5 reduction of adherence compared to the NT group, considering the previously performed T12 experiment with equal setup to the planned 3.0Ag a similar log 0.5 reduction at $p < 0.001$ significance was seen for adherence compared to NT, despite 2 instead of 3 implants analysed for adherence and a similar ± log 1 reduction for the bacteria in the media after the experiment. At a log 0.5 reduction for the silver treated implants compared to the NT controls this suggest barely any effect of the AgNPs in these dynamic conditions.

Despite limited data differences and comparisons between this and static adherence could be determined. Starting with the log 1 ($p < 0.05$) adherence reduction between NT and 0.3Ag for the static assay which is very comparable to the dynamic's log 0.5 reduction ($p < 0.05$). Subsequent NT-3.0Ag comparison does however give a big difference between static and dynamic conditions, near zero adherence for the static experiment ($p < 0.001$) was measured against a 0.5 log reduction ($p < 0.001$) of the dynamic assay which indicate a lesser antibacterial effect in the dynamic assay. Such difference of the dynamic reactor could be due to dispersion of ions released from the implant interface, preventing locally rising concentration of released of ions as measured by ICP-OES and thus reducing the region in which the implants were able to inhibit bacterial growth as seen in the ZOI assays.

As addition to the adherence measured by CFU, qualitative SEM imaging of some of the rescued implants were adapted as additional check of the conclusions based on the CFU measurements. For the static implants near homogenously distributed bacteria were adhering after incubation, here the NT implant had the least apparent adherence on its relatively smooth surface, compared to the other groups where despite antibacterial properties on 0.3Ag and 3.0Ag implants a similar spread occurred on the PEO implant. SEM imagining is but a qualitative measurement, especially when performed without duplicates, however, finding close to zero adherence for the 3.0Ag implants by CFU assay yet having a similar visual adherence on each of the PEO treated implant groups weakens the CFU based

conclusion. Such results could occur with bacteria adhering to the internal implant porosities invisible for SEM visualisation, by extended period of storage between sample collection and visualisation or could have been an unrepresentative implant. On sonicated implants of the static assay bacteria could no longer be spotted, which indicate that the bacteria were successfully removed from the implant surface to a degree where the removed bacteria were still viable as measured for the respective implants. Implants collected from the dynamic experiments displayed differences between the groups, such as bacteria clustering on NT implant, biofilm initiation on the PEO implant and adherence solely occurring in implant cavities for the 0.3Ag implant. After sonication, the implants were expected to be cleared of adherent bacteria similar to what was seen for the static implants, such that the number of removed bacteria could be measured. Implants of the dynamic experiment, however, displayed homogenic spread of adherent bacteria over their surface after sonication, which was surprisingly also seen on the 0.3Ag implant despite no surface adherence on the un-sonicated sample. Whether this is observed due to having encountered an unrepresentative implant, swapping implants during remote implant handling or due to effect related to the dynamic environment can be indefinitely discussed but will at this point remain uncertain.

Continuing the initiated chain of growth of biofilm on the non-sonicated implants would be quite viable with the clustering and biofilm initiation seen on the implants. Converting the methodology to one that forms mature biofilms would require an additional incubation in nutrient rich media. Followed by SEM analysis for this group of biofilm covered implants.

4.4 Research limitations

Despite duplicate experiments for most assays, the data recovered was objectively lacking in terms of power. In hindsight and without hindrance of COVID-19 some would have already been repeated while others provided insight in how to prevent such limitations in next studies.

Among the experiments which would have been repeated, were the ICP-OES silver release, which had measurement errors where 0 Ag release was found for all 3 samples of the 6h time point of the 0.3Ag group. Here the control of Ca release was within expectancy, and at the previous (3h) and later (12h) time points non-zero silver release was measured, indicating that this was indeed an assay-side error. As the 3h and 12h release gave ranges of expectant release, the assay still provided confidence in silver release comparable to that of previous implants.

For ZOI design changes were made concerning bacterial strain, number of bacteria, timing of placement and implant size. With these changes due to logistic limitations and in-house methodology, an exact reproduction was unavailable. Instead the assay was performed such that comparison between high, low and no silver PEO treated implants could be made. Thus, despite being unable to directly compare the ZOI methodology between this and the previous PEO related studies, the high and low silver concentrations both showed antibacterial properties for this study.

Without exact fluid flow or subsequent fluid shear stresses known at the bone surface, the relation to the determined shear stresses is limited. For the stresses in the bone porosities such as the vascular or lacunar-canalicular systems the interstitial fluid could however reach substantially greater flow rates due to small channel dimensions this was in previous research studied and expected to be occurring within the 0.8 and 3 Pa range [51]. Further research would be required to further pinpoint the shear stresses on bone surface, which would validate the models' dynamics.

Bioreactor experiments were performed in series due to a single reactor available, instead performing the experiments simultaneously in parallel with exactly similar inoculum, if possible, in the same reactor omitting as much variables as possible would improve the power of the experiment outcomes. As this was not logistically feasible for the current setup, some pragmatic, but less than ideal design

choices such as static experiments performed in a different geometric environment (wells plates), dynamic experiments split in a series cause a loss of strength. With loss of inoculum accuracy as one of these aspects caused by the time between experiments, a consistent method to have more direct control over inoculum concentration, such as OD measurements could be another potential upgrade if this can be optimized to fit the bacteria strain and inoculum concentrations. These together with the zero measurements at t20, indicate that methodological optimization is very much possible and could with model improvements increase the strength of consequent results. Similarly, to further increase accuracy of measurements and inoculum concentrations, CFU count could have been performed more aggressively, using more agar plates when out of the 30-300 bounds. Despite storing all important aliquots for later use, they were only later analysed to be of interest when measurements could no longer be performed due to COVID-19.

Despite the qualitative nature of imagining by SEM, in the case of observations where samples with low visible adherence had high measured CFU or the other way around this weakens the argument of the measurements found by CFU and requires repetition. With a repetition of the SEM imagines or having performed these in duplicate, which would have been performed had all experiments continued, the observations could be checked for consistency and would eliminate potential processing errors.

Even though most of the experiments were concluded, the procedures related to COVID-19 still caused a gap in the research data and hindered the study. Experiments had been finished with preliminary readouts collected, however, the adherence measurements, verification of surprising results by duplicates or re-plating, SEM preparation of the implants, verification of sonication process and the setup of an additional bacterial behaviour analysis by QPCR were all lost or simply unavailable.

Chapter 5 Conclusions

This study aimed to determine whether the dynamic conditions' shear flow influenced the antibacterial effect of the different PEO treatments in the prevention of bacterial adherence compared to their antibacterial effects displayed in static conditions.

A comparison of the implants of this study to those studied in previous works was determined by implant characterisation. Despite slight differences in the ZOI assay, the similar results in EDS surface analysis, silver ion release and SEM topology review provided evidence that the obtained implants were comparable to those used in the previous studies. Clear antibacterial effect of the silver for the 3.0g/l group together with the minor effect seen for the 0.3 g/l group validates the antibacterial effect of silver on these implants, similar to the antibacterial effects seen in previous work.

The release of silver ions over time was analysed, with the lower release of ions found for less-silver incorporated implants. In the dynamic bioreactor the released ions were dispersed and mixed throughout the media due to the fluid flow, decreasing the local ion concentration. Earlier analysed antibacterial effect such as the ZOI assay displayed a clear local effect attributed to these silver ions. An ion concentration decrease would intuitively decrease the antibacterial effect, as was seen in the available adherence results but not further confirmed by the pre-sonication SEM analysis.

An experimental setup, such as this custom bioreactor setup should be capable of providing robust and consistent outcomes. This model, despite its optimization trials and troubleshooting, still intermittently encountered zero values in media measurements at 20h during the experiments. This rejects the robustness and consistency of the custom bioreactor setup and promotes the need for its optimization prior to follow-up experiments. How and why this behaviour occurred remains unsolved, with suspected causes remaining; the difference glass reactor vessels, due to the "non-zero, zero, non-zero, zero" pattern in t20 bacteria concentration, the aspects previously analysed during the model optimization, or due to the pressure put on the bacteria by the stirring dynamics. Neither of these, however, could be pinpointed as cause for a total loss of bacteria in the runs where this occurred.

The dynamic environment of the bioreactor is generated by stirring the fluid at constant speed, introducing flow and shear stresses on the implants. These shear stresses were simulated within a modelled stirred bioreactor, from which the peak and average shear stress were calculated along the implants. Comparing these to the *in vivo* shear conditions the simulated average stresses were as low as those in intracellular fluid.

To recap, antibacterial biomaterials, such as the titanium implants incorporated with silver nano particles by PEO, present a frontier in the prevention of bacterial adherence, the formation of biofilm, and the consequential infections with all their further complications. In prior research these implants have been studied in *ex vivo* and *in vitro* experiments where positive and sufficient results were analysed on antibacterial effect in static conditions. With the patients' body consisting of varying dynamics, this study analysed whether the antibacterial biomaterial's efficacy is sufficient to prevent adherence in dynamic conditions as could be expected *in vivo*. Despite the incomplete data set, the CFU results imply that more adherence occurred in the generated dynamic conditions, exposing the implants to shear stresses like those encountered in interstitial fluid, compared to the static experiments. These effects were visually analysed on SEM imagining after the experiment and before sonication, the images were however unable to confirm this effect. These findings provide insight and direction and critical aspects for improvements and direction for further research towards additional analysis of adherence in dynamic conditions, with the successful development of clinically applicable novel biomaterials as the goal.

Chapter 6 Further research

During the thesis work valuable steps towards deeper understanding of the bacterial adherence in dynamic conditions, the mechanism in play and limitations were found, continuation on this understanding and offsetting the limitations are key points to take into account in future research.

Alterations of the CDC bioreactor caused occasional lack of bacteria in the media after the experiment. This seemingly random complete disappearance has a cause, which is not yet pinpointed. Most likely this effect is due to lower nutrient content in combination with the stirring, which could be too much pressure for the bacteria. Why this did not occur every experiment is both the most interesting and challenging question. Another, quite unlikely, yet probable cause potentially adding to the pressure of the stirring would be a slight difference in the glass reactor vessels. The difference between runs, and the pattern of it occurring would seem like occasionally every other day the problems arise, but this would not answer why some runs were consequently successful, or unsuccessful.

Variability seen in the dynamic model, answered or not, could potentially be prevented or offset when the different groups are performed in parallel or in the same reactor with additional analysis of media and conditions at hourly intervals. When logistically possible, this approach could remove inter-experimental variance and allow direct comparison between groups.

Simulated flow dynamics and shear conditions were similar to those in intracellular fluid, however this only considered the shear force aspect analysed in the CFD. To analyse the true dynamics, and simultaneously validate the simulated model, fluid dynamics such as flow speed should be additionally studied for the model. Additionally, considering the flow dynamics and the increase of adherence due to the expected dispersion of silver ion, it is equally interesting to analyse whether this decrease in concentration is accompanied by higher release of silver ions due to the shear forces similarly introduced. As silver release was currently measured in static conditions, it would instead be studied in the bioreactor model at the same dynamics as experienced during bacterial adherence. Ion release would then be studied during (non-)bacterial run(s) with measuring instruments able to determine ion content in the media of the reactor, or at aliquots despite the diluted concentrations.

Lab logistics, troubleshooting of the experimental model and the COVID-19 closure of research facilities caused some planned experiments to fall out of the scope of the study. Despite their omissions these are relevant experiments to be considered. Repeating the experiments with a gram-negative *Pseudomonas aeruginosa* strain was one of these experiments and would provide an excellent addition to the gram-positive Staphylococcus Aureus. For better understanding of the local antibacterial effect due to the ion release a virulence study was theorized to analyse the *Staphylococcus aureus* virulence factors by QPCR after contact with the different implants at static and dynamic conditions. Additionally, for the custom bioreactor setup which focuses on adherence, an additional incubation step in nutrient rich media is required to achieve mature biofilm. This is however yet to be analysed for this model and would be evaluated by repeating the adherence experiment with Ti-6Al-4V discs where after removal of the remnant fluid and non-adherent bacteria these would undergo an additional incubation in the reactor with TSB as media instead of PBS. Biofilm growth facilitated by this method would subsequently be analysed by SEM imaging after rinsing the implants and dehydration similar to the bacterial adherence assays. Prior to the dehydration an additional step of fixation would be performed by a 15 min drench in PBS containing 4% Paraformaldehyde and 1% Glutaraldehyde to preserve the biofilm structure.

In future studies with optimized adherence or biofilm models a start should be made with as little variation between experiments as possible. For *in vitro* biomaterial research and development work where such models are used for, the translation of variables and parameters of the model to more *in vivo* like conditions provides results and differences which previously, without animal or human trials

might not have been observed. Such variable parameters and inputs are for instance the temperature, flow dynamics, implant placements, media additives (such as serum, albumin, nutrients or plasma), working with additional bacterial stems or animal-/human cells and finally coculturing these. All these aspects which when logistically, financially and pragmatically feasible, elevate a model to new heights with the aim and holy grail being an *in vitro* co-culture model in which all aspects related to the implant site are considered, allowing *in vitro* development and preliminary validation of novel products, reducing costs, development times and limiting animal and human trials to the essential validations.

Chapter 7 References

[1] M. Colilla, I. Izquierdo-Barba, M. Vallet-Regi, The Role of Zwitterionic Materials in the Fight against Proteins and Bacteria, Medicines (Basel) 5(4) (2018). https://10.3390/medicines5040125.

[2] M.M.J. Nielen, M.J.J.C. Poos, A.M. Gommer, F.F. Jager, Artrose naar type in 2018, 01-05-2020. https://www.volksgezondheidenzorg.info/onderwerp/artrose/cijfers-context/huidige-situatie#node-prevalentie-en-aantal-nieuwe-gevallen-van-artrose-huisartsenpraktijk. (2020).

[3] M.H.D. Plasmans, V.R. Ramjiawan, R.A.A. Vonk, Zorguitgaven artrose naar type 2017, 28-10-2019. https://www.volksgezondheidenzorg.info/onderwerp/artrose/kosten/zorguitgaven#node-zorguitgaven-artrose-naar-leeftijd-en-geslacht. (2020).

[4] Dutch Arthroplasty Register (LROI), Online LROI annual report 2019. https://www.lroi-rapportage.nl/. (2020).

[5] L. Yuan, S. Ding, C. Wen, Additive manufacturing technology for porous metal implant applications and triple minimal surface structures: A review, Bioact Mater 4(1) (2019) 56-70. https://10.1016/j.bioactmat.2018.12.003.

[6] M. Wang, T. Tang, Surface treatment strategies to combat implant-related infection from the beginning, Journal of orthopaedic translation 17 (2019) 42-54. https://10.1016/j.jot.2018.09.001.

[7] L. Tian, N. Tang, T. Ngai, C. Wu, Y. Ruan, L. Huang, L. Qin, Hybrid fracture fixation systems developed for orthopaedic applications: A general review, Journal of orthopaedic translation 16 (2019) 1-13. https://10.1016/j.jot.2018.06.006.

[8] A. Radtke, M. Ehlert, T. Jedrzejewski, M. Bartmanski, The Morphology, Structure, Mechanical Properties and Biocompatibility of Nanotubular Titania Coatings before and after Autoclaving Process, J Clin Med 8(2) (2019). https://10.3390/jcm8020272.

[9] A. Przekora, Current Trends in Fabrication of Biomaterials for Bone and Cartilage Regeneration: Materials Modifications and Biophysical Stimulations, Int J Mol Sci 20(2) (2019). https://10.3390/ijms20020435.

[10] M. Moravej, D. Mantovani, Biodegradable metals for cardiovascular stent application: interests and new opportunities, Int J Mol Sci 12(7) (2011) 4250-70. https://10.3390/ijms12074250.

[11] H.B.M. Hilderink, M.J.J.C. Poos, A.M. Gommer, Toekomstige trend artrose door demografische ontwikkelingen. https://www.volksgezondheidenzorg.info/onderwerp/artrose/cijfers-context/trends#node-toekomstige-trend-artrose-door-demografische-ontwikkelingen. (2020).

[12] Z.Z. Akanda, M. Taha, H. Abdelbary, Current review-The rise of bacteriophage as a unique therapeutic platform in treating peri-prosthetic joint infections, Journal of orthopaedic research : official publication of the Orthopaedic Research Society 36(4) (2018) 1051-1060. https://10.1002/jor.23755.

[13] A.J. Tande, R. Patel, Prosthetic joint infection, Clin Microbiol Rev 27(2) (2014) 302-45. https://10.1128/CMR.00111-13.

[14] C.R. Arciola, D. Campoccia, G.D. Ehrlich, L. Montanaro, Biofilm-based implant infections in orthopaedics, Advances in experimental medicine and biology 830 (2015) 29-46. https://10.1007/978-3-319-11038-7_2.

[15] A.C. Rothenberg, A.E. Wilson, J.P. Hayes, M.J. O'Malley, B.A. Klatt, Sonication of Arthroplasty Implants Improves Accuracy of Periprosthetic Joint Infection Cultures, Clinical orthopaedics and related research 475(7) (2017) 1827-1836. https://10.1007/s11999-017-5315-8.

[16] M.M. Kheir, T.L. Tan, C. Higuera, J. George, C.J. Della Valle, M. Shen, J. Parvizi, Periprosthetic Joint Infections Caused by Enterococci Have Poor Outcomes, The Journal of arthroplasty 32(3) (2017) 933-947. https://10.1016/j.arth.2016.09.017.

[17] A. Trampuz, A.F. Widmer, Infections associated with orthopedic implants, Curr Opin Infect Dis 19(4) (2006) 349-56. https://10.1097/01.qco.0000235161.85925.e8.

[18] M.R. Kiedrowski, A.R. Horswill, New approaches for treating staphylococcal biofilm infections, Ann N Y Acad Sci 1241 (2011) 104-21. https://10.1111/j.1749-6632.2011.06281.x.

[19] M. Chen, H. Sun, H. Ouyang, J.E. Jones, Q. Yu, Y. Xu, S. Revu, Biofilm-inhibiting and Osseointegration-promoting Orthopedic Implants with Novel Nanocoatings, (2020). https://doi.org/10.1007/978-3-030-34471-9_3.

[20] I.A.J. van Hengel, M. Tierolf, V.P.M. Valerio, M. Minneboo, A.C. Fluit, L.E. Fratila-Apachitei, I. Apachitei, A.A. Zadpoor, Self-defending additively manufactured bone implants bearing silver and copper nanoparticles, J Mater Chem B 8(8) (2020) 1589-1602. https://10.1039/c9tb02434d.

[21] I.A.J. van Hengel, N.E. Putra, M. Tierolf, M. Minneboo, A.C. Fluit, L.E. Fratila-Apachitei, I. Apachitei, A.A. Zadpoor, Biofunctionalization of selective laser melted porous titanium using silver and zinc nanoparticles to prevent infections by antibiotic-resistant bacteria, Acta Biomater (2020). https://10.1016/j.actbio.2020.02.044.

[22] I.A.J. van Hengel, M. Riool, L.E. Fratila-Apachitei, J. Witte-Bouma, E. Farrell, A.A. Zadpoor, S.A.J. Zaat, I. Apachitei, Selective laser melting porous metallic implants with immobilized silver nanoparticles kill and prevent biofilm formation by methicillin-resistant Staphylococcus aureus, Biomaterials 140 (2017) 1-15. https://10.1016/j.biomaterials.2017.02.030.

[23] G.A. Van Norman, Drugs, Devices, and the FDA: Part 2: An Overview of Approval Processes: FDA Approval of Medical Devices, JACC Basic Transl Sci 1(4) (2016) 277-287. https://10.1016/j.jacbts.2016.03.009.

[24] Y. Yuan, D. Lin, F. Chen, C. Liu, Clinical translation of biomedical materials and the key factors towards product registration, Journal of orthopaedic translation 2(2) (2014) 49-55. https://10.1016/j.jot.2013.12.002.

[25] D. Novianar, S. Estuningsih, M.F. Ulum, Animal Study and Pre-clinical Trials of Biomaterials, 2016. https://10.1007/978-3-319-14845-8_4

[26] S. Saeidnia, A. Manayi, M. Abdollahi, From in vitro Experiments to in vivo and Clinical Studies; Pros and Cons, Current Drug Discovery Technologies 12(4) (2016) 218-224. https://10.2174/1570163813666160114093140.

[27] Center for Devices and Radiological Health (CDRH),

Medical Device Innovation Initiative White Paper, 10/31/2017. https://www.fda.gov/about-fda/cdrh-innovation/medical-device-innovation-initiative-white-paper. (2020).
[28] D.M. Goeres, L.R. Loetterle, M.A. Hamilton, R. Murga, D.W. Kirby, R.M. Donlan, Statistical assessment of a laboratory method for growing biofilms, Microbiology 151(Pt 3) (2005) 757-762. https://10.1099/mic.0.27709-0.
[29] D.L. Williams, S.R. Smith, B.R. Peterson, G. Allyn, L. Cadenas, R.T. Epperson, R.E. Looper, Growth substrate may influence biofilm susceptibility to antibiotics, PloS one 14(3) (2019) e0206774. https://10.1371/journal.pone.0206774.
[30] R.M. Rasmussen, R.T. Epperson, N.B. Taylor, D.L. Williams, Plume height and surface coverage analysis of methicillin-resistant Staphylococcus aureus isolates grown in a CDC biofilm reactor, Biofouling 35(4) (2019) 463-471. https://10.1080/08927014.2019.1612381.
[31] D.M. Goeres, D.K. Walker, K. Buckingham-Meyer, L. Lorenz, J. Summers, B. Fritz, D. Goveia, G. Dickerman, J. Schultz, A.E. Parker, Development, standardization, and validation of a biofilm efficacy test: The single tube method, J Microbiol Methods 165 (2019) 105694. https://10.1016/j.mimet.2019.105694.
[32] D.L. Williams, K.L. Woodbury, B.S. Haymond, A.E. Parker, R.D. Bloebaum, A modified CDC biofilm reactor to produce mature biofilms on the surface of peek membranes for an in vivo animal model application, Curr Microbiol 62(6) (2011) 1657-63. https://10.1007/s00284-011-9908-2.
[33] D.M. Goeres, M.A. Hamilton, N.A. Beck, K. Buckingham-Meyer, J.D. Hilyard, L.R. Loetterle, L.A. Lorenz, D.K. Walker, P.S. Stewart, A method for growing a biofilm under low shear at the air-liquid interface using the drip flow biofilm reactor, Nat Protoc 4(5) (2009) 783-8. https://10.1038/nprot.2009.59.
[34] R. Ferrer-Espada, X. Liu, X.S. Goh, T. Dai, Antimicrobial Blue Light Inactivation of Polymicrobial Biofilms, Front Microbiol 10 (2019) 721. https://10.3389/fmicb.2019.00721.
[35] D. Ausbacher, L. Lorenz, B. Pitts, P.S. Stewart, D.M. Goeres, Paired methods to measure biofilm killing and removal: a case study with Penicillin G treatment of Staphylococcus aureus biofilm, Lett Appl Microbiol 66(3) (2018) 231-237. https://10.1111/lam.12843.
[36] ASTM, ASTM E2562 - 17, Standard Test Method for Quantification of Pseudomonas aeruginosa Biofilm Grown with High Shear and Continuous Flow using CDC Biofilm Reactor, West Conshohocken, PA, 2017, www.astm.org, ASTM International, 2017.
[37] ASTM, ASTM E3161 - 18, Standard Practice for Preparing a Pseudomonas aeruginosa or Staphylococcus aureus Biofilm using the CDC Biofilm Reactor, West Conshohocken, PA, 2018, www.astm.org, ASTM International, 2018.
[38] S.J. Kim, J. Chang, B. Rimal, H. Yang, J. Schaefer, Surface proteins and the formation of biofilms by Staphylococcus aureus, Biochim Biophys Acta Biomembr 1860(3) (2018) 749-756. https://10.1016/j.bbamem.2017.12.003.
[39] K.M. Thompson, N. Abraham, K.K. Jefferson, Staphylococcus aureus extracellular adherence protein contributes to biofilm formation in the presence of serum, FEMS Microbiol Lett 305(2) (2010) 143-7. https://10.1111/j.1574-6968.2010.01918.x.
[40] P. Neopane, H.P. Nepal, R. Shrestha, O. Uehara, Y. Abiko, In vitro biofilm formation by Staphylococcus aureus isolated from wounds of hospital-admitted patients and their association with antimicrobial resistance, Int J Gen Med 11 (2018) 25-32. https://10.2147/IJGM.S153268.
[41] Mixer Application, COMSOL Multiphysics® v. 5.4., COMSOL AB, Stockholm, Sweden, 2018.
[42] H.F. George, F. Qureshi, Newton's Law of Viscosity, Newtonian and Non-Newtonian Fluids, in: Q.J. Wang, Y.-W. Chung (Eds.), Encyclopedia of Tribology, Springer US, Boston, MA, 2013, pp. 2416-2420. https://10.1007/978-0-387-92897-5_143
[43] J. Vaithilingam, R.D. Goodridge, R.J.M. Hague, S.D.R. Christie, S. Edmondson, The effect of laser remelting on the surface chemistry of Ti6al4V components fabricated by selective laser melting, Journal of Materials Processing Technology 232 (2016) 1-8. https://10.1016/j.jmatprotec.2016.01.022.
[44] J. Moering, Improving eds elemental analysis situ experiments, 2017. https://www.protochips.com/blog/improving-eds-elemental-analysis-situ-experiments/. (2020).
[45] G.J. Humphreys, A.J. McBain, An Introduction to the Biology of Biofilm Recalcitrance, 2014. https://doi.org/10.1016/B978-0-12-397043-5.00014-1
[46] J.P. Chandy, M.L. Angles, Determination of nutrients limiting biofilm formation and the subsequent impact on disinfectant decay, Water Research 35(11) (2001) 2677-2682. https://10.1016/s0043-1354(00)00572-8.
[47] H. Kanematsu, M.D. Barry, Formation and Control of Biofilm in Various Environments, 2020. http://10.1007@978-981-15-2240-6
[48] B.F. Gilmore, T.M. Hamill, D.S. Jones, S.P. Gorman, Validation of the CDC biofilm reactor as a dynamic model for assessment of encrustation formation on urological device materials, J Biomed Mater Res B Appl Biomater 93(1) (2010) 128-40. https://10.1002/jbm.b.31567.
[49] J.J. Paszkowiak, A. Dardik, Arterial wall shear stress: observations from the bench to the bedside, Vasc Endovascular Surg 37(1) (2003) 47-57. https://10.1177/153857440303700107.
[50] D.E. Conway, S.G. Eskin, L.V. McIntire, Effects of Mechanical Forces on Cells and Tissues (The Liquid–Cell Interface), Biomaterials Science2013, pp. 474-487. https://10.1016/b978-0-08-087780-8.00040-1
[51] C. Wittkowske, G.C. Reilly, D. Lacroix, C.M. Perrault, In Vitro Bone Cell Models: Impact of Fluid Shear Stress on Bone Formation, Front Bioeng Biotechnol 4 (2016) 87. https://10.3389/fbioe.2016.00087.